Petrogenetic relationships and assimilation processes in the alkalic Iron Mask batholith, south-central British Columbia

L.D. SNYDER and J.K. RUSSELL
Department of Geological Sciences, Mineral Deposit Research Unit
The University of British Columbia, Vancouver, British Columbia

ABSTRACT

The Lower Jurassic Iron Mask batholith intrudes Upper Triassic Nicola Group volcanic rocks in the Quesnellia terrane of south-central British Columbia and hosts Cu-Au mineralization. The batholith comprises three mappable intrusive phases, including: Pothook gabbro to diorite, Cherry Creek monzodiorite to monzonite and Sugarloaf diorite. The Iron Mask hybrid forms a fourth mappable unit that makes up to 45% of the areal exposure in the batholith. It is highly variable in texture and composition and subdivided into three types; Type I and II have abundant (partially digested) xenoliths, many of which are derived from the Nicola Group, whereas Type III is xenolith-poor and shows extreme outcrop-scale textural diversity.

Pothook and Cherry Creek rocks are similar in texture, mineralogy, whole rock and mineral composition and style of alteration. Contacts between the two can be intrusive or gradational. Rocks collected from these two suites have compositions that are permissive of a single magma batch, although simple crystal fractionation does not explain all chemical variations within and between the two suites. The Sugarloaf unit comprises a diverse group of amphibole-phyric rock types and is texturally and mineralogically distinct from Pothook and Cherry Creek suites.

The Iron Mask hybrid represents progressive stages of physical and chemical interaction between Nicola Group country rocks and Pothook magma. Magmatic assimilation (selective or partial) is supported on the basis of field relationships, petrographic observations, and REE compositional data. Thermal dehydration and partial assimilation of Nicola Group rocks by Pothook magma is shown to be a valid means of promoting early and extensive volatile saturation in the Iron Mask batholith.

Introduction

The Iron Mask batholith, located in the Quesnellia terrane of the southern Intermontane Belt (Fig. 1), is one of several Early Jurassic (205 ± 4 Ma; Mortensen et al., this volume) alkalic intrusions in British Columbia. Porphyry style Cu-Au mineralization is found throughout the batholith (Carr and Reed, 1976; Ross et al., this volume; Lang and Stanley, this volume); the Afton, Ajax, Crescent and Pothook deposits have all produced significant quantities of these metals (Kwong, 1987; Ross et al., this volume). The Iron Mask batholith also hosts vein style magnetite/apatite lode deposits (Cann, unpub.).

This paper describes and characterizes the intrusive rock types comprising the Iron Mask batholith with respect to texture, mineralogy, and chemical composition. Based on these data, intrusive relationships between several of the major rock types are reinterpreted. Furthermore, the magmatic origins of these rocks are re-examined in terms of their cogenetic relationships and the role of assimilation in the formation of the "Iron Mask hybrid": an enigmatic unit which crops out over a significant portion of the batholith. We anticipate that this analysis will provide a sounder basis from which to understand the individual porphyry Cu-Au deposits within the batholith, described elsewhere in this volume.

Regional Geology

The Iron Mask batholith is located approximately 10 km southwest of the city of Kamloops and is accessible via major thoroughfares and abundant secondary ranching and mining roads. This area is characterized by an arid climate and consists mainly of broad, rolling hills which are dominated by sagebrush and sparse pine forest vegetation. Bedrock exposure is poor, especially in the southern portion of the Iron Mask batholith.

The Iron Mask batholith intrudes Upper Triassic Nicola Group rocks which comprise an areally extensive (70 km by 190 km) and thick (7000 m) package of volcanic, volcaniclastic and related sedimentary rocks distributed across the Quesnellia terrane (Schau, 1970; Preto, 1977, 1979; Mortimer, 1987). Nicola Group rocks have been interpreted to represent a volcanic arc sequence accreted onto the western margin of North America in the Middle Jurassic (Monger et al., 1982; Monger, 1989a). They have been subdivided by Preto (1977) into three distinct, sub-parallel, north-trending belts. The Iron Mask batholith intrudes rocks of either the Eastern or Central Nicola volcanic belt, which are broadly folded and regionally metamorphosed to zeolite, prehnite-pumpellyite, and greenschist facies (Preto, 1977; Mortimer, 1987).

Adjacent to the Iron Mask batholith, Nicola Group rocks consist of green to purple coloured basaltic and andesitic clinopyroxene-phyric flows and flow breccias, light green massive tuffs, and green andesitic to dacitic bedded ash to lapilli tuffs. Minor amounts of hematitic, poorly bedded chert and dark grey plagioclase-phyric flows and dikes are also present. Nicola Group rocks are commonly foliated near the margin of the batholith and copper mineralization is observed in many outcrops (Cockfield, 1948; Carr, 1956). Picritic basalt is found outside the western margin of the batholith near Jacko Lake and north of Kamloops Lake (Mathews, 1941; Cockfield, 1948; Carr, 1956; Preto, 1967; Snyder and Russell, 1993, 1994).

The Iron Mask batholith intrudes Nicola Group rocks along deep-seated structures (Preto, 1967; Northcote, 1974, 1976, 1977). It consists of two separate masses: (1) the northwest trending 5 km by 20 km Iron Mask batholith in the south, and (2) the smaller (5 km by 5 km) Cherry Creek pluton to the north (Fig. 2). Contacts between the Iron Mask batholith and Nicola Group are either faulted (on the eastern margin), intrusive (observed along the western contact) or not exposed. Locally, Nicola Group rocks are hornfelsed up to 50 m from intrusive contacts and recrystallized clasts of Nicola origin are found within Iron Mask rock units, being particularly abundant along the western margin. Larger lenses of sheared, altered and metamorphosed Nicola Group rocks are also present, especially in mineralized areas (Ross et al., 1993; Stanley,

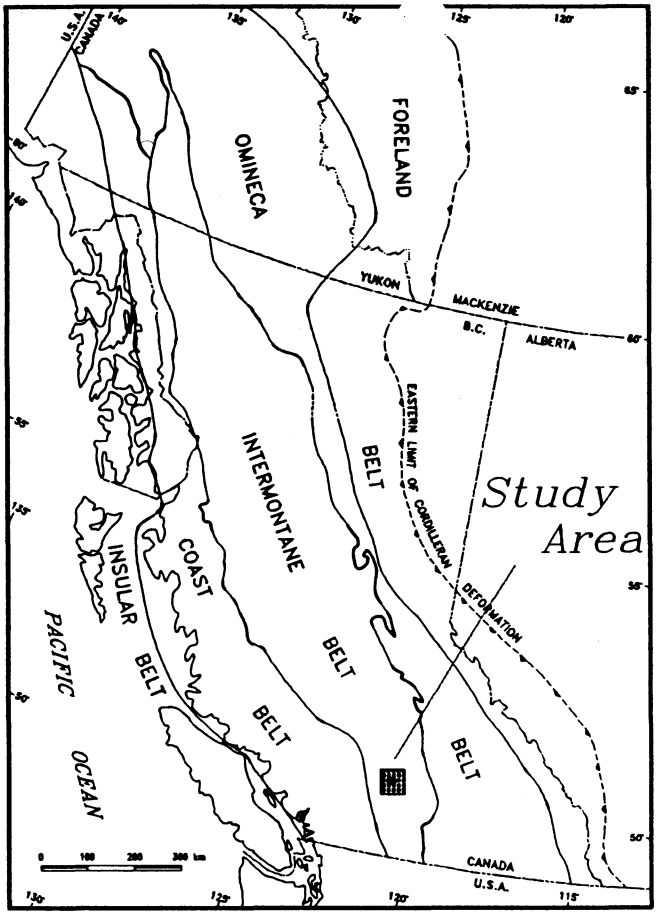

FIGURE 1. Location map for the Iron Mask batholith within the Intermontane Belt of the Canadian Cordillera, south-central British Columbia.

1994). The association be[illegible]n mineralization and large pods of country rock may reflect either common control along permeable shear zones or bias imposed by extensive mapping around mineralized zones.

Eocene Kamloops Group volcanic rocks are exposed as small, flat-lying erosional remnants atop the Iron Mask batholith and within an east-west trending graben which separates the batholith from the Cherry Creek pluton (Fig. 2; Northcote, 1977; Ewing, 1982; Kwong, 1987). The Kamloops Group consists dominantly of alkali olivine basalt flows with minor intercalated sedimentary rocks (Ewing, 1981a, 1981b). Kwong (1987) reports small exposures of other Tertiary volcanic rocks within the Iron Mask pluton.

Rock Types In The Iron Mask Batholith

Many of the previous stratigraphic columns established for the Iron Mask batholith and related rocks are shown in Table 1. This paper, based on Snyder and Russell (1993), revises or clarifies age relationships between several intrusive rock units and postulates different origins for several map units (Table 1). Mathews (1941) and Cockfield (1948) were the first to describe the geology of the Iron Mask batholith (Table 1). Later, more extensive petrologic descriptions were provided by Carr (1956), Preto (1967, 1972) and Hoiles (1978), while emphasizing the mineral deposits potential and exploration activities within the batholith. Northcote (1974, 1976, 1977) remapped the batholith and documented the major textural and mineralogical characteristics of the intrusive rock units. Kwong (1987) produced the latest geological map for the Iron Mask batholith, compiling an extensive amount of data from past workers.

The Iron Mask batholith comprises three distinct intrusive rock types (Fig. 2) including, from oldest to youngest, gabbro and diorite belonging to the Pothook phase, Cherry Creek monzodiorite to monzonite and the Sugarloaf diorite (Table 1, Snyder and Russell, 1993). The Iron Mask batholith also contains a complex rock unit characterized by abundant partially digested xenoliths and extreme compositional and textural variability. Previous workers considered this diverse map unit as part of the batholith (e.g., Mathews, 1941;

TABLE 1. Summary of past and current revised intrusive relationships established for plutonic and related rocks of the Iron Mask batholith (IMB), which incorporates information from past workers Mathews (1941), Cockfield (1948), Carr (1956), Carr and Reed (1976), Preto (1967), Northcote (1977), Hoiles (1978), Cann (1979), Kwong (1987) and Monger, (1989b). Ancillary notes to each stratigraphic column are keyed by number.

(1) Mathews (1941) Cockfield (1948)	(2) Carr (1956)	(3) Preto (1967) Livingstone (1960)	(4) Carr & Reed (1976)	(5) Northcote (1977)	(6) Hoiles (1978)	(7) Revised Snyder & Russell (1993)
	IMB	**Post - IMB**	**IMB**	**IMB**	**IMB**	**IMB**
		a) Cherry Creek	Cherry Creek	Cherry Creek	Cherry Creek	Sugarloaf
		b) Sugarloaf	Sugarloaf	Sugarloaf	(4 types)	
IMB	diorite to syenite		Picrite			
(syenite to peridotite)	(fine-grained)			Picrite (?)	Sugarloaf	Cherry Creek
				Pothook	Picrite	
	gabbro to syenite	**IMB**				
	(coarse-grained)	a) diorite to monzonite	Pothook and IM units (gabbro to diorite)	IM hybrid	Pothook (gabbro to diorite) IM unit	Pothook/Hybrid
		b) gabbro to syenite				
	Picrite	Picrite				Picrite
Nicola Group	Nicola Group	Nicola Group	Nicola Group	Nicola Group	Nicola Group	Nicola Group

1. IMB is viewed as a single differentiated (syenite to peridotite) magma; ultramafic rocks intrude Nicola Group and are related to the IMB.
2. Picrite is viewed as intrusive but not batholithic and correlated with picrites north of Kamloops Lake; picrite was emplaced between coarser and finer-grained intrusions.
3. Cherry Creek rocks are mainly porphyries and breccias associated with alteration and mineralization.
4. Picrite is intrusive and emplaced between Pothook and Sugarloaf.
5. Extended the definition of Cherry Creek and noted conflicting age relationships between Cherry Creek and Sugarloaf intrusions. Picrite origin and age are unresolved: views picrite as intrusive but not related to IMB. Notes that Pothook can be gradational between IM hybrid and Cherry Creek and that IM hybrid incorporates Nicola Group rocks.
6. Picrite thought to intrude Nicola Group rocks (Jacko Lake) and to be structurally part of IMB but with unresolved genetic relationship.
7. Sugarloaf replaces Cherry Creek as youngest magmatic phase (cf. "conflicting relationships" of Northcote, 1977). Cherry Creek rocks show a strong chemical affinity to Pothook rocks, probably indicating a genetic linkage. Pothook diorite is genetically linked to hybrid rocks, which derive from assimilation of Nicola Group rocks (cf. Northcote, 1977). Picrite basalts are pre-Iron Mask, arc-related ultramafic volcanic rocks, unrelated to IMB.

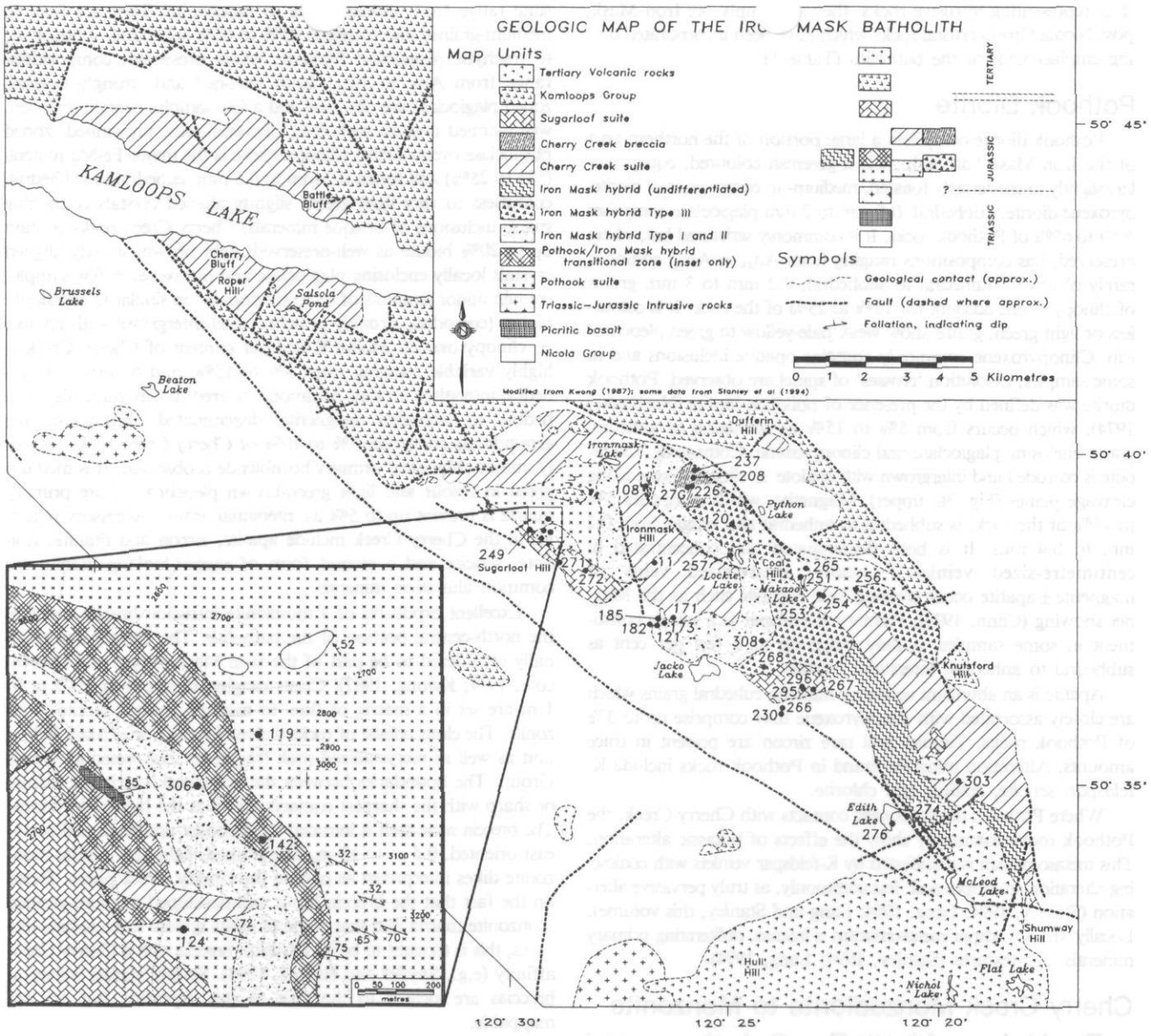

FIGURE 2. Geological map of the Iron Mask batholith. Map units, distributions of rock types and contact relationships are from Snyder and Russell (1993) and Snyder (1994) and incorporate observations and modified interpretations of Mathews (1941), Cockfield (1948), Northcote (1977), Preto (1967), Kwong (1987) and Stanley et al. (1994). Inset (Snyder and Russell, 1993) illustrates the transitional zone between the Pothook suite and the Iron Mask hybrid unit (Type II).

Cockfield, 1948; Carr, 1956; Preto, 1967) and later (e.g., Northcote, 1977) named it the Iron Mask hybrid unit. It was identified as an agmatite: a migmatite structure derived solely from the brecciation of pre-existing metamorphic rocks by magma, wherein breccia fragments experience minimal transport and can be rejoined without gaps (Mehnert, 1971). The 'Iron Mask hybrid' is retained herein as a mappable unit, although a strictly 'agmatite' origin is ruled out for the majority of the unit. Hybrid rocks are interpreted to be coeval with intrusion of the Pothook diorite (Snyder and Russell, 1993; Stanley et al., 1994).

Lenses of serpentinized picritic basalt up to 250 m in exposed length are scattered throughout the Iron Mask batholith. These ultramafic rocks were thought at one time to be cogenetic with the Iron Mask batholith (e.g., Cockfield, 1948). Later workers established that the picrites were not part of the batholith proper and were perhaps associated with ultramafic rocks exposed north of Kamloops Lake (Carr, 1956; Preto, 1967; Carr and Reed, 1976). However, the picrites and serpentinized equivalents were still considered to be intrusive and more often than not were considered coeval to Iron Mask plutonism (e.g., Carr and Reed, 1976; Northcote, 1977). As late as Hoiles (1978) and Kwong (1987), the picrites remained problematic in terms of their origins. For example, Monger (1989b) correlated occurrences of picritic basalt, outside the batholith near Jacko Lake and on the north side of Kamloops Lake near Watching Creek and Carabine Creek (Cockfield, 1948; Snyder and Russell, 1993, 1994), with the Iron Mask intrusive suite, based on the occurrence of serpentinite lenses and pods in the batholith.

Most recently, Snyder and Russell (1994) demonstrated that the serpentinized picrite basalts within the Iron Mask are equivalent to the ultramafic volcanic rocks exposed at Jacko Lake and at the several localities north of Kamloops Lake, based on mineralogy, mineral chemistry, and major, trace and REE whole rock compositions. They demonstrated that these volcanic rocks represent arc-derived ultramafic volcanic rocks, situated stratigraphically above the Nicola Group, and that they are unrelated to the Iron Mask batholith rocks. Whereas, Hoiles (1978) interpreted the picrite at Jacko Lake to be intruding Nicola Group rocks, the authors suggest that the picrites are stratigraphically conformable to and overlying Nicola Group. Lastly, the most logical explanation for the serpentinite occurrences within the Iron Mask batholith is that, rather

than representing intrusive rocks, they ε nply pre-Iron Mask, post-Nicola Group crustal rocks which have been incorporated during emplacement of the batholith (Table 1).

Pothook Diorite

Pothook diorite comprises a large portion of the northern part of the Iron Mask batholith. It is a greenish coloured, equigranular, slightly to moderately foliated, medium- to coarse-grained biotite-pyroxene diorite. Subhedral, 0.5 mm to 2 mm plagioclase comprises 40% to 65% of Pothook rocks. It is commonly sericitized but, where preserved, has compositions ranging from An_{43} to An_{52}; zoning is rarely observed. Euhedral to subhedral, 0.2 mm to 3 mm grains of clinopyroxene account for 15% to 25% of the rock. It is colourless or light green; grains show weak pale-yellow to green pleochroism. Clinopyroxene commonly contains opaque inclusions and in some samples, exsolution 'crosses' of spinel are observed. Pothook diorite was defined by the presence of poikilitic biotite (Northcote, 1974), which occurs from 5% to 15% as subhedral to anhedral grains enclosing plagioclase and clinopyroxene. Commonly, the biotite is corroded and intergrown with epidote ± clinopyroxene along cleavage planes (Fig. 3a, upper). Magnetite, which comprises 5% to 15% of the rock, is subhedral to anhedral and ranges from 0.2 mm to 0.4 mm. It is both disseminated and concentrated in centimetre-sized veinlets. Locally, metre-sized veins of magnetite ± apatite occur creating lode deposits such as the Magnet showing (Cann, 1979). Primary K-feldspar is a minor constituent in some samples; it may range up to a few per cent as subhedral to anhedral, interstitial crystals.

Apatite is an abundant accessory mineral; euhedral grains which are closely associated with clinopyroxene may comprise up to 3% of Pothook rocks. Titanite and rare zircon are present in trace amounts. Alteration minerals found in Pothook rocks include K-feldspar, sericite, epidote and chlorite.

Where Pothook diorite is near contacts with Cherry Creek, the Pothook rocks commonly show the effects of potassic alteration. This metasomatism is manifested by K-feldspar veinlets with coalescing alteration envelopes and, less commonly, as truly pervasive alteration (Stanley, 1994; Lang, 1994; Lang and Stanley, this volume). Locally, the K-feldspar metasomatism is intense, obliterating primary minerals and textures (Stanley, 1994; Lang, 1994).

Cherry Creek Monzodiorite to Monzonite

The original usage of the term Cherry Creek unit was restricted to a suite of intermediate to felsic porphyritic intrusions, dikes, and breccias of the Iron Mask batholith (Preto, 1967; 1972). Later workers (e.g., Northcote, 1977) extended the definition of the unit to include a more diverse assemblage of dioritic to syenitic rocks within the main part of the batholith (e.g., Kwong, 1987). Hoiles (1978), for example, recognized four classes of Cherry Creek rocks including: breccias, porphyries, syenite to monzonite trachytes, and non-porphyritic, medium to fine-grained diorites.

Separation of Cherry Creek-like rocks from those having a Pothook affinity is a non-trivial task given their mineralogical and compositional similarities. The task is complicated further by the manifestation of pervasive, extreme potassium metasomatism of Pothook and Cherry Creek phases along their contacts (Lang, 1994). The work of Lang (1994), Lang and Stanley (this volume) and Stanley et al. (1994), for example, suggests that much of the 'Cherry Creek syenite' could derive, in fact, from extensive metasomatism of Pothook rocks and other Cherry Creek phases, with the consequence that previous maps of the batholith have tended to overrepresent Cherry Creek and underestimate Pothook rocks (e.g., Kwong, 1987).

In assigning rocks to either the Pothook or Cherry Creek suite the authors have tried to be consistent with and to reconcile this literature. For example, where possible, the authors have assigned rocks to the Pothook suite based on the presence of poikilitic biotite. In the authors' study, the rocks assigned to the Cherry Creek suite range from monzc te to monzonite. They are fine- to medium-grained and comprise 45% to 65% subhedral, subtrachytic to trachytic plagioclase feldspar; where preserved, compositions range from An_{35} to An_{45}. Both unzoned and strongly normal-zoned plagioclase are observed and a few samples contain unzoned, well-twinned crystals with thin, discontinuous, untwinned, zoned plagioclase overgrowths. Clinopyroxene is the major Fe-Mg mineral (5% to 25%) and forms 0.2 mm to 0.5 mm, euhedral to subhedral, colourless to very light green, slightly aligned crystals containing sparse inclusions of opaque minerals. Cherry Creek rocks contain up to 20% biotite as well-preserved, light brown, weakly aligned crystals locally enclosing plagioclase and pyroxene. A few samples contain minor amounts of a second population similar to 'Pothook' biotite (corroded, strongly poikilitic, and intergrown with epidote ± clinopyroxene). Modal K-feldspar content of Cherry Creek is highly variable, ranging from 3% to 15%, and occurring as anhedral interstitial crystals commonly altered to clay minerals. Subhedral to anhedral magnetite disseminated throughout the groundmass comprises 5% to 10% of Cherry Creek rocks. Locally, minor chloritized primary hornblende is observed. It is medium green in colour and light green-brown pleochroic. Rare primary quartz is present up to 5% as interstitial grains. Accessory minerals in the Cherry Creek include apatite, zircon and titanite. Epidote, sericite and a second form of ragged-looking titanite are common alteration minerals.

Excellent exposures of a monzonite intrusion breccia occur in the north-central portion of the batholith. The breccia was originally considered to be part of the Iron Mask hybrid unit (Northcote, 1977; Kwong, 1987). Clasts ranging in size from 0.03 m to 1 m are set in a matrix of fine- to medium-grained biotite monzonite. The clasts consist of rocks derived from the Iron Mask hybrid unit as well as recrystallized rock fragments interpreted as Nicola Group. The boundaries between the clasts and matrix are diffuse or sharp with the sharpest contacts found at the higher elevations. The breccia zone itself is intruded by abundant northwest and northeast oriented, 0.5 m to 15 m, fine-grained, light grey biotite monzonite dikes interpreted as part of the Cherry Creek phase. Based on the fact that the breccia has a well-developed medium-grained monzonite matrix and that some of clasts appear to be hybrid-like rocks, this is thought to be an intrusion breccia with a Cherry Creek affinity (e.g., Snyder and Russell, 1993). Several similar intrusion breccias are located to the west of this exposure, but are not mappable.

Sugarloaf Diorite

The Sugarloaf unit comprises a suite of hornblende-phyric dioritic rocks exposed as lenticular bodies and dikes in the western part of the batholith and in the adjacent Nicola Group. Rocks of the Sugarloaf phase are distinctive for their porphyritic nature, manifest in abundant, locally trachytic phenocrysts of amphibole in a fine-grained groundmass. Locally, subhedral to anhedral phenocrysts of plagioclase are present.

Sugarloaf diorite contains 25% to 55%, euhedral to subhedral, 0.5 mm to 1 mm plagioclase grains (locally trachytic) which are commonly altered to sericite or saussurite. Where preserved, plagioclase has compositions ranging from An_{32} to An_{38}. Amphibole, commonly altered to chlorite, makes up 15% to 55% of the rock as euhedral to subhedral, locally aligned crystals up to 1.5 cm in length. Amphibole commonly replaces clinopyroxene (e.g., Preto, 1967) which occurs as 0.5 mm rounded, corroded grains. Magnetite is present in minor amounts as euhedral to subhedral grains up to 0.5 mm. Rarely, primary K-feldspar comprises up to 10% of Sugarloaf rocks.

Accessory minerals in Sugarloaf rocks include apatite, titanite and rare quartz. Secondary minerals include epidote, chlorite and minor calcite. The secondary K-feldspar occurs rarely as small veinlets, large poikilitic grains, and interstitial grains. Albitization is the most prominent style of alteration in Sugarloaf rocks and is espe-

cially intense near mineralized zones [illegible] and Stanley, this volume). At the Ajax East pit, secondary albite has destroyed much of the original texture (Ross et al., 1993; Ross et al., this volume).

Iron Mask Hybrid

The Iron Mask hybrid unit accounts for approximately 45% of the mappable exposure of the Iron Mask batholith. It is mineralogically and texturally diverse and is subdivided on the basis of texture and clast abundance into three main types. Type I Iron Mask hybrid is confined to thin (50 m to 75 m) discontinuous zones along contacts between the Iron Mask batholith and the Nicola Group. It is an intrusive breccia characterized by abundant (60% to 80%) angular fragments which are themselves derived from immediately adjacent Nicola Group. Matrix in Type I hybrid is fine- to medium-grained pyroxene hornblende diorite. Type II Iron Mask hybrid is characterized by abundant xenoliths (10% to 80%) of volcanic, plutonic and recrystallized sedimentary rocks (Fig. 3b, middle). This heterolithic variety is exposed near the margins of Pothook dioritic stocks in the western and central portions of the batholith. Within Type II hybrid, the clasts have reacted to varying degrees with the enclosing magma. Some clasts are angular with sharp boundaries whereas others are rounded with more diffuse boundaries (e.g., plagioclase crystals span xenolith-matrix interfaces). The igneous matrix of Type II is texturally variable on an outcrop scale. In many areas the matrix consists predominantly of fine- to coarse-grained interlocking, randomly-oriented grains of pyroxene, biotite, plagioclase, euhedral magnetite and rare hornblende. In other locations, it consists of fine- to medium-grained, trachytic hornblende and plagioclase with euhedral magnetite and lesser amounts of subhedral pyroxene and subhedral to anhedral biotite. Modal mineralogy is characteristically non-uniform and locally the matrix is anorthositic.

Type III Iron Mask hybrid dominates the northeastern portion of the batholith. These rocks have fewer (< 10%) xenoliths which are generally highly recrystallized and digested. Type III hybrid varies from fine-grained to almost pegmatitic on an outcrop scale with pods and dikelets of different compositional and textural characteristics distributed randomly. Modal mineral proportions vary greatly between outcrops, however, there is some relationship between grain size and mineralogy. Coarser-grained patches in Type III are characterized by subhedral, equant grains of clinopyroxene and plagioclase with disseminated coarse magnetite. The clinopyroxene is commonly chloritized and rimmed by dark brown amphibole. Locally, some coarser-grained rocks contain trachytic, acicular megacrysts (up to 15 cm in length) of amphibole which enclose clinopyroxene and plagioclase. Trachytic hornblende and normally-zoned plagioclase with lesser amounts of pyroxene and disseminated magnetite are found in finer-grained material.

In places Type III hybrid is texturally and compositionally homogeneous over areas of approximately 250 m. These zones are either coarse or fine-grained and each contains distinctive, internally consistent mineral assemblages. At their margins, these homogenous patches grade into more typical Type III rocks where outcrop-scale textural and compositional heterogeneity dominates (e.g., Coal Hill, Fig. 2).

Accessory minerals are apatite and rare titanite and zircon. Primary K-feldspar is absent, although areas of faint K-feldspar overprinting near contacts with the Cherry Creek suite have been observed. Secondary minerals in the Iron Mask hybrid rocks include chlorite, epidote and hornblende overgrowths on clinopyroxene.

Contact Relationships

Contacts between Pothook diorite and the Type II Iron Mask hybrid can be gradational as noted by Northcote (1977). Figure 2 (inset) shows in detail the gradational nature of the Pothook - Iron Mask Type II Hybrid transition over a 50 m to 250 m wide zone (Snyder and Russell, 1993). Across the transitional unit from

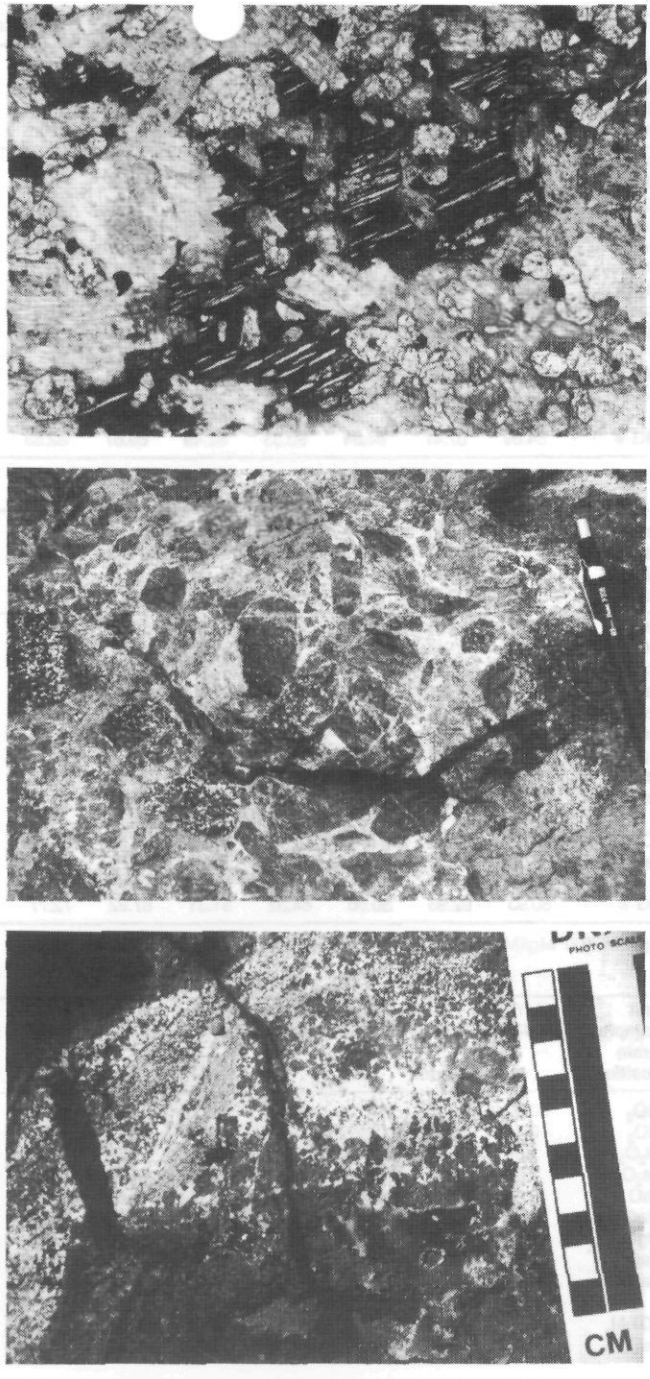

FIGURE 3. Photomicrograph and outcrop photographs of Iron Mask rocks showing: (A, upper plate) poikilitic biotite (4 mm to 5 mm) found throughout Pothook diorite (field of view is 5 mm), (B, middle plate) outcrop- to handsample-scale characteristics of Type II Iron Mask hybrid involving recrystallized and partially digested xenoliths, and (C, lower plate) incomplete assimilation of Nicola group rocks common to the hybrid unit.

Pothook into the Iron Mask hybrid, on the north slope of Sugarloaf Hill, the following changes occur (Snyder and Russell, 1993; Stanley et al., 1994). Pothook diorite incorporates clasts of plutonic, volcanic and recrystallized sedimentary rocks while the characteristic magnetite veining and weak foliation of this rock unit become less prominent. Rounded and partially digested and disaggregated xenoliths increase in abundance and magnetite occurs as discrete euhedral to subhedral grains in the matrix. The Pothook matrix varies from fine to medium grained on a scale of several centimetres and mineralogical heterogeneity is manifest by zones of dominantly felsic or mafic minerals. Finally, poikilitic biotite, characteristic of Pothook intrusive rocks, disappears as hornblende increases. Con-

TABLE 2. Representative electron ;roprobe analyses of clinopyroxene fro. arious Iron Mask rocks

Unit	PH	PH	PH	PH	PH	PH	PH	PH	PH	PH	PH-TZ	PH-TZ	CC	CC	CC	CC
Sample	IM-251	IM-251	IM-119	IM-119	IM-257	IM-257	IM-265	IM-265	IM-124	IM-124	IM-242	IM-242	IM-237	IM-237	IM-171	IM-171
Grain	2	1	2	6	1	1	4	4	3	2	4	5	11	6	3	7
Position	Core	Rim	Int	Core	Rim	Int	Rim	Int	Core	Core	Int	Int	Core	Core	Int	Rim
SiO_2	49.34	50.27	51.46	52.89	51.98	52.97	52.20	53.33	52.36	53.54	51.57	52.05	53.04	51.88	51.00	52.02
TiO_2	0.57	0.57	0.30	0.23	0.20	0.02	0.18	0.19	0.26	0.00	0.24	0.11	0.20	0.20	0.14	0.13
Al_2O_3	3.88	2.64	1.42	1.12	1.22	0.24	1.23	0.69	1.05	0.60	0.94	0.60	0.92	0.94	1.36	0.63
Fe_2O_3	3.67	3.44	2.42	2.33	1.59	1.34	1.79	2.14	2.94	1.72	3.49	4.06	1.40	3.15	2.92	2.81
FeO	4.47	3.82	4.63	2.93	5.49	3.24	5.68	2.44	4.18	2.11	3.96	1.22	5.77	3.99	6.23	4.83
MnO	0.36	0.49	0.43	0.30	0.56	0.42	0.70	0.49	0.32	0.00	0.60	0.27	0.81	0.80	0.68	0.75
MgO	13.87	14.95	14.51	15.43	14.51	15.87	15.04	16.55	14.99	16.30	14.67	15.88	14.90	14.92	14.70	15.17
CaO	21.92	21.80	22.35	23.75	22.28	23.81	21.44	23.46	22.50	24.59	22.65	23.87	22.49	22.64	20.28	22.04
Na_2O	0.41	0.38	0.49	0.50	0.41	0.20	0.42	0.32	0.61	0.30	0.47	0.43	0.36	0.40	0.44	0.32
TOTAL	98.49	98.36	98.01	99.48	98.24	98.11	98.68	99.61	99.21	99.16	98.59	98.49	99.89	98.92	97.75	98.70
FeO(T)	7.77	6.92	6.81	5.03	6.92	4.45	7.29	4.37	6.83	3.66	7.10	4.87	7.03	6.82	8.86	7.36
MG #	84.69	87.47	84.84	90.33	82.49	89.67	82.53	92.36	86.49	93.24	86.81	95.87	82.15	86.95	80.80	84.83

Unit	CC	CC	CC	CC	CC	CC	CC	CC	CC	CC	dike	dike	dike	dike	dike	dike
Sample	IM-303	IM-303	IM-27G	IM-27G	IM-253	IM-253	IM-11	IM-11	IM-269	IM-269	IM-254	IM-254	IM-208	IM-208	IM-308	IM-308
Grain	3	4	5	6	7	5	9	8	3	2	1	5	1	5	5	5
Position	Int	Rim	Rim	Core	Int	Int	Int	Int	Rim	Rim	Rim	Int	Rim	Rim	Int	Core
SiO_2	52.91	49.34	52.16	51.72	51.52	50.79	51.76	52.24	52.59	49.96	52.09	51.80	52.69	50.89	49.85	52.78
TiO_2	0.13	0.44	0.34	0.26	0.34	0.37	0.13	0.13	0.19	0.18	0.15	0.16	0.21	0.24	0.35	0.17
Al_2O_3	0.70	2.15	1.74	1.32	1.75	1.71	0.97	0.80	0.92	0.85	0.79	0.89	1.54	1.48	2.50	1.14
Fe_2O_3	0.69	5.21	1.09	2.88	1.29	4.18	1.47	1.98	1.41	5.33	1.92	3.10	0.89	3.59	3.49	1.76
FeO	6.16	2.04	6.18	4.73	5.74	3.53	8.14	5.22	5.74	1.96	5.45	3.85	5.81	3.06	5.09	2.39
MnO	0.75	0.45	0.82	0.69	0.80	0.70	1.14	0.65	0.89	0.79	0.91	0.94	0.66	0.73	0.37	0.18
MgO	14.65	15.05	14.34	14.81	13.98	14.40	12.20	14.73	14.47	14.73	14.44	15.16	14.67	14.76	13.26	17.20
CaO	22.41	22.12	21.93	22.12	21.33	22.50	22.50	22.38	22.19	22.43	22.38	22.27	22.40	22.82	22.49	22.89
Na_2O	0.36	0.38	0.44	0.42	0.68	0.51	0.47	0.39	0.48	0.47	0.36	0.38	0.41	0.38	0.44	0.16
TOTAL	98.76	97.18	99.04	98.95	97.43	98.69	98.78	98.52	98.88	96.70	98.49	98.55	99.28	97.95	97.84	98.98
FeO(T)	6.78	6.73	7.16	7.32	6.90	7.29	9.46	7.00	7.01	6.76	7.18	6.64	6.61	6.29	8.23	3.97
MG #	80.93	92.93	80.56	84.82	81.31	87.92	72.77	83.43	81.80	93.04	82.52	87.53	81.83	89.55	82.30	92.75

Mg# = $100*Mg/(Mg + Fe^{2+})$ TZ = Pothook/Hybrid Transitional Zone

Unit	HY-I	HY-I	HY-II	HY-II	HY-III	HY-III	HY-III	HY-III	HY-XE	HY-XE	HY-XE	HY-XE	SL	SL	SL	SL
Sample	IM-173	IM-173	IM-306	IM-306	IM-120	IM-120	IM-256	IM-256	IM-121	IM-121	IM-268	IM-268	IM-274	IM-274	IM-272	IM-272
Grain	2	1	8	3	7	6	6	6	4	3	6	1	2	2	1	2
Position	Int	Rim	Int	Int	Rim	Int	Int	Rim	Int	Int	Core	Int	Rim	Rim	Int	Int
SiO_2	50.96	50.70	51.71	50.25	49.80	48.50	50.78	51.35	50.81	49.92	48.53	50.25	50.63	52.01	53.05	48.95
TiO_2	0.44	0.42	0.27	0.44	0.62	0.78	0.58	0.44	0.39	0.40	0.70	0.66	0.29	0.13	0.06	0.38
Al_2O_3	2.84	2.97	1.90	2.23	3.78	4.32	2.65	2.61	3.04	3.29	4.88	3.68	2.36	1.08	0.20	3.00
Fe_2O_3	2.95	4.15	2.28	4.65	2.92	4.94	3.22	4.47	2.73	4.36	4.16	3.61	2.80	2.73	0.90	4.56
FeO	3.98	2.85	5.06	2.94	4.28	2.65	4.26	1.66	3.59	2.38	3.41	2.35	5.24	1.26	6.14	4.58
MnO	0.31	0.28	0.48	0.43	0.33	0.30	0.36	0.33	0.20	0.14	0.18	0.21	0.40	0.12	0.21	0.63
MgO	14.92	15.06	15.31	15.37	14.42	14.16	14.83	15.14	15.16	15.12	13.77	14.90	14.27	17.08	13.97	13.36
CaO	22.41	22.87	21.40	21.84	21.87	22.39	22.14	23.11	22.66	22.99	22.62	23.72	21.85	23.31	24.21	21.91
Na_2O	0.38	0.38	0.40	0.38	0.39	0.40	0.40	0.70	0.28	0.25	0.34	0.26	0.38	0.14	0.27	0.39
TOTAL	99.19	99.68	98.81	98.53	98.41	98.44	99.22	99.81	98.86	98.91	98.59	99.64	98.22	98.07	99.01	97.82
FeO(T)	6.63	6.58	7.11	7.12	6.91	7.10	7.16	5.68	6.05	6.30	7.15	5.60	7.76	3.72	6.95	8.68
MG #	86.97	90.43	84.37	90.34	85.77	90.55	86.12	94.22	88.26	91.91	87.83	91.84	82.97	96.05	80.21	83.90

tacts between the Pothook and Cherry Creek rocks are locally ambiguous. In many areas, especially in the northern part of the batholith, extreme K-feldspar metasomatism has rendered identification uncertain. Further ambiguity arises through apparently contrasting intrusive relationships between Cherry Creek rocks and the coeval Pothook unit. For example, near Makaoo Lake in the central part of the batholith coarse-grained, foliated Pothook diorite has a gradational contact with medium to fine-grained, non-foliated pyroxene-monzodiorite of the Cherry Creek unit over a distance of approximately 100 m (Snyder and Russell, 1993). There is no evidence suggesting that Pothook rocks are younger than the Cherry Creek phases; conversely, Lang (1994) has described the presence of Cherry Creek-like dikes brecciating the Pothook phase in the Crescent pit.

This apparent temporal overlap between Cherry Creek rocks and the Pothook and Iron Mask hybrid units is permissible. For example, if the Iron Mask hybrid unit formed by interactions between Pothook magma and Nicola Group country rocks, it would likely occupy the top and sides of the batholith, forming a relatively brittle shell around hotter, deeper uncontaminated Pothook magma. At this time, a phase of the Cherry Creek unit could intrude and brecciate the hybrid carapace while simultaneously mingling and interacting with unsolidified Pothook magma at depth.

Snyder and Russell (1993) addressed the question of which intrusive phase is the youngest in the Iron Mask batholith. They concluded that dikes assigned to the Sugarloaf suite are observed to cross-cut Nicola Group, picrite basalt and serpentinite, Pothook diorite and Iron Mask hybrid. The Sugarloaf suite is construed to be younger than the Cherry Creek unit because Cherry Creek has ambiguous contact relationships with Pothook phase which is itself demonstrably older than Sugarloaf suite. In actual fact, there is probably little temporal difference between the times of emplacement of the Pothook, Cherry Creek and Sugarloaf intrusive suites (cf. Northcote, 1977; Snyder and Russell, 1993).

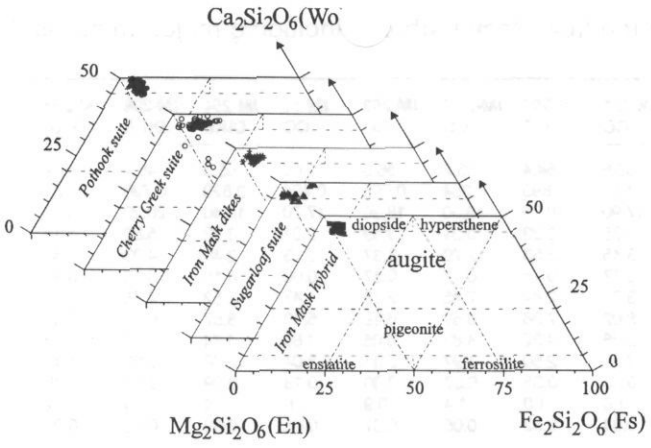

FIGURE 4. Pyroxene quadrilateral showing clinopyroxene compositions for all major phases of the Iron Mask batholith.

Clinopyroxene Compositions

Clinopyroxene is the most common Fe-Mg mineral in most rocks of the Iron Mask batholith. In Pothook and Cherry Creek rocks, pyroxene occurs as colourless to light green, subhedral grains. The Iron Mask hybrid unit contains dominantly greenish-coloured clinopyroxene in both the matrix as well as the recrystallized xenoliths whereas Sugarloaf rocks locally contain rounder, colourless clinopyroxene.

Green-coloured clinopyroxene is a common phase in mafic alkaline rocks (Scott, 1976; Brooks and Printzlau, 1978; Barton and van Bergen, 1981) and can serve as a useful petrogenetic indicator (Bedard et al., 1988). For example, tholeiitic, calc-alkaline and alkaline rock suites can be distinguished on the basis of Al^{IV} contents of clinopyroxene (LeBas, 1962). Clinopyroxene compositions are useful in tracking the extent of fractionation (Scott, 1976). Zoning patterns in clinopyroxene have been used to recognize magmatic contamination or infer changes in pressure and temperature (e.g., Bedard et al., 1988). Compositions of clinopyroxene from rocks of the Iron Mask batholith were measured by electron microprobe (EMP) for major and minor elements and used to investigate magmatic linkages within and between intrusive phases.

Analytical Methods and Results

All compositions were measured with the Cameca SX-50 electron microprobe at The University of British Columbia. Individual grains were analyzed with a focussed, spot-fixed beam at operating conditions of 15 kV and 20 nA and peak counting times of 30 seconds. Background concentrations were counted for 10 seconds. Calibration standards included: diopside (Si, Mg, Ca), aegirine (Fe, Na), grossularite (Al), pyromangite (Mn), rutile (Ti), chromite (Cr) and nickel-olivine (Ni).

Representative clinopyroxene analyses from rocks in the Iron Mask batholith are shown in Table 2. Chromium was analyzed for, but found at levels below detection in most samples. Clinopyroxene compositions, on the whole, span a narrow compositional range (Fig. 4); pyroxene from Cherry Creek rocks plot as diopside to augite, whereas pyroxene from other units are diopsidic (Morimoto, 1989). Calculated Mg#'s range from 73 to 96. Iron Mask pyroxene contains significant amounts of calculated Fe_2O_3 (0.7 - 5.2 wt%) based on charge balance considerations (e.g., 4 cations and 6 oxygens).

Clinopyroxene from Pothook diorite has Mg#'s ranging from 82.5 to 98.1; core to rim zoning averages 3 Mg units. In over half the analyses (n = 111), pyroxene from Pothook rocks had insufficient Al (0.25 - 3.88 wt% Al_2O_3) to fill the tetrahedral site vacancies. Figure 5a shows Pothook rocks to be relatively depleted in Al^{IV} compared to clinopyroxene from Sugarloaf rocks and the

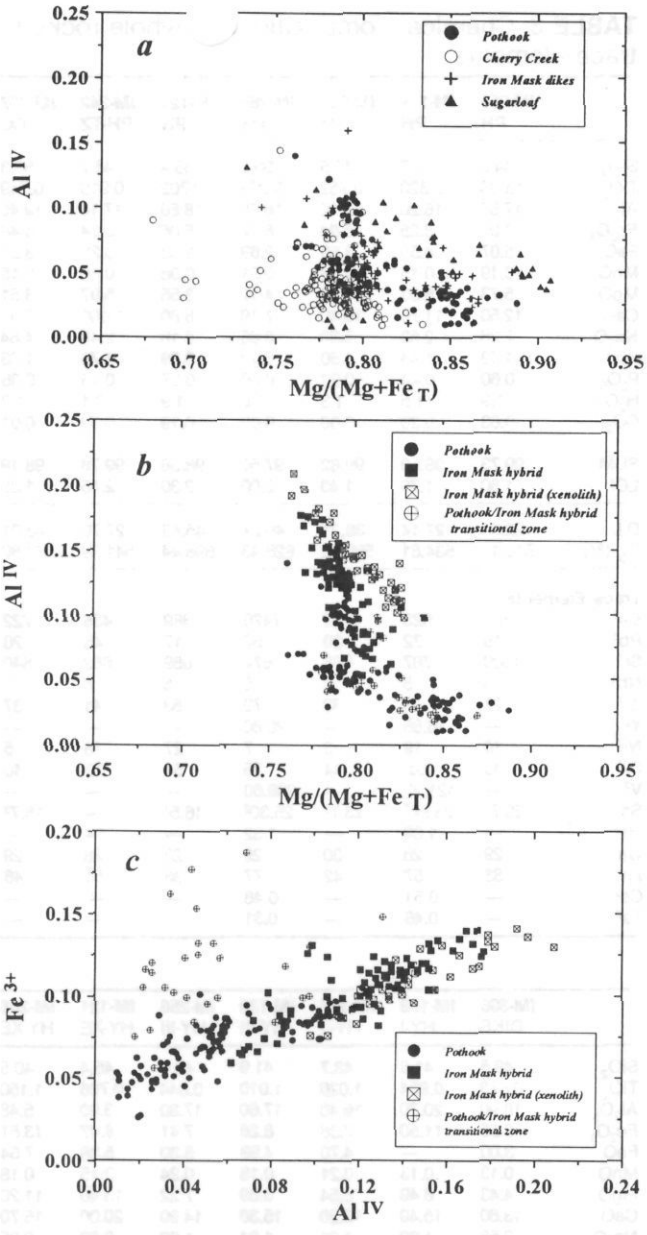

FIGURE 5. Clinopyroxene compositions from the Iron Mask batholith plotted as: (A, B) Al^{IV} vs $Mg/[Mg+Fe_T]$, and (C) Al^{IV} vs calculated Fe^{3+}.

Iron Mask dikes. However, most clinopyroxene from Cherry Creek rocks, although showing lower Mg#'s (72.8 to 92.9) and less zoning (2 Mg units from core to rim), are similar in Al^{IV} content. Again over half of the pyroxene analyses from Cherry Creek rocks show tetrahedral site deficiencies, implying tetrahedrally-coordinated Ti^{4+} or Fe^{3+} (Bedard et al., 1988; Cundari and Salviulo, 1989). TiO_2 concentrations in Pothook clinopyroxene range from below detection to 0.64 wt% and in Cherry Creek grains from 0.02 - 0.47 wt%.

Clinopyroxene compositions from Sugarloaf rocks have Mg#'s of 80 to 96 and show a stronger chemical zonation (6 Mg units) probably reflecting the hypabyssal nature of these rocks. Al^{IV} contents of Sugarloaf pyroxene are slightly higher (Fig. 5a), although 11 out of 33 analyzed grains have tetrahedral site vacancies. Lastly, Sugarloaf pyroxene compositions have less Fe_T and greater Cr_2O_3 ($\leq$0.56 wt%) than does pyroxene from Pothook or Cherry Creek rocks.

Clinopyroxene from the Iron Mask hybrid has high Mg#'s (86 to 94), shows little zoning (2.7 Mg units) and has Si and Al^{IV}-filled tetrahedral sites (Fig. 5b). TiO_2 concentrations are higher than

TABLE 3. Chemical composition, whole rocks from the Iron Mask batho, including major, minor and trace elements

	IM-251 PH	IM-119 PH	IM-257 PH	IM-265 PH	IM-124 PH	IM-242 PH-TZ	IM-237 CC	IM-171 CC	IM-303 CC	IM-27G CC	IM-253 CC	IM-11 CC	IM-254 DIKE	IM-208 DIKE	IM-226 DIKE
SiO_2	44.8	45.7	49.5	50.2	50.4	46.7	50.3	52.6	54.4	55.2	56.5	61.0	55.3	46.4	50.9
TiO_2	1.030	0.820	0.752	0.832	0.702	0.910	0.749	0.919	0.693	0.654	0.656	0.404	0.629	0.796	0.887
Al_2O_3	17.50	16.20	19.10	16.70	18.50	17.10	19.40	17.90	18.70	18.30	18.30	17.70	18.40	20.20	19.00
Fe_2O_3	7.07	8.25	5.04	6.77	5.06	6.84	4.48	3.75	3.23	3.34	3.39	2.01	3.73	5.82	5.11
FeO	5.07	4.55	3.50	2.69	2.82	3.20	3.28	3.45	3.53	2.70	2.37	2.13	2.40	4.03	3.40
MnO	0.19	0.15	0.19	0.21	0.08	0.16	0.15	0.17	0.14	0.12	0.17	0.09	0.18	0.18	0.20
MgO	5.73	5.03	4.36	4.12	3.55	5.97	3.51	3.87	2.84	2.45	2.18	1.47	2.52	4.35	3.67
CaO	12.50	11.70	10.40	7.19	8.80	12.00	9.08	8.02	7.36	6.57	6.19	5.13	6.57	10.90	8.44
Na_2O	2.28	2.53	3.60	3.65	5.10	2.48	4.64	3.86	4.32	4.83	5.05	4.80	4.74	3.23	4.53
K_2O	1.03	1.44	1.50	3.10	0.89	1.76	1.03	2.27	2.50	1.97	3.31	3.04	2.70	0.93	1.41
P_2O_5	0.60	0.44	0.32	0.39	0.37	0.15	0.36	0.33	0.35	0.37	0.30	0.18	0.29	0.65	0.39
H_2O^+	1.9	1.5	1.3	1.6	1.9	2.1	1.2	1.6	1.0	1.4	0.9	1.0	1.4	1.4	1.2
CO_2	0.03	0.20	0.06	0.05	0.19	0.39	0.01	0.04	0.32	0.05	0.07	0.06	0.02	0.03	0.08
SUM	99.73	98.50	99.62	97.50	98.36	99.76	98.19	98.78	99.39	97.95	99.38	99.02	98.88	98.92	99.22
LOI	1.80	1.70	1.40	2.00	2.30	2.45	1.25	1.65	1.45	1.70	1.00	1.45	1.45	1.45	1.50
D.I.	22.81	27.14	36.21	46.27	45.48	27.70	43.01	44.66	49.89	56.05	60.30	73.65	55.42	30.53	43.60
T_{Zr} (°C)	519.12	534.61	560.53	628.43	598.44	541.39	584.80	625.45	634.33	639.98	657.26	670.98	651.25	550.54	590.01
Trace Elements															
Ba[1]	643	523	1182	1420	389	435	722	990	1250	1130	1340	1700	1355	1220	1600
Rb[1]	19	32	30	52	17	45	20	40	43	33	54	37	47	21	29
Sr[1]	1080	787	985	674	689	652	840	798	756	679	731	597	647	1330	961
Nb[1]	6	5	4	5	5	6	7	4	8	7	8	5	6	6	5
Zr[1]	27	40	33	79	53	41	37	65	62	59	86	72	79	24	41
Y[2]	—	16.85	—	20.80	—	—	—	—	20.60	19.94	—	15.47		—	—
Ni[1]	10	19	3	7	27	18	5	7	b.d.	9	b.d.	6	2	3	b.d.
Cr[1]	33	b.d.	44	25	54	27	40	28	24	b.d.	20	22	23	26	25
V[2]	—	421.23	—	289.60	—	—	—	—	206.62	177.40	—	119.81	—	—	—
Sc	30.7[3]	25.94[2]	23.7[3]	25.30[2]	16.5[3]	—	16.7[3]	20.6[3]	13.24[2]	10.43[2]	9.2[3]	5.81[2]	8.8[3]	16.8[3]	18.5[3]
Hf[2]	—	1.09	—	1.32	—	—	—	—	0.97	0.82	—	1.26	—	—	—
Ga[1]	29	28	30	29	28	28	29	29	29	29	30	30	28	29	30
Zn[1]	83	57	42	77	36	51	48	69	43	42	55	35	62	65	59
Cs[2]	—	0.51	—	0.48	—	—	—	—	0.80	0.39	—	0.42	—	—	—
Ta[2]	—	0.48	—	0.31	—	—	—	—	0.57	0.75	—	1.19	—	—	—

	IM-308 DIKE	IM-173 HY-I	IM-306 HY-II	IM-120 HY-III	IM-256 HY-III	IM-121 HY-XE	IM-268 HY-XE	IM-267 SL	IM-271 SL	IM-296 SL	IM-274 SL	IM-272 SL	IM-266 SL	IM-295 SL	IM-249 SL
SiO_2	49.5	41.8	43.7	41.9	42.0	45.4	40.5	48.1	48.7	50.0	50.5	51.8	52.3	52.5	54.5
TiO_2	0.878	0.954	1.020	1.010	0.844	0.706	1.150	0.820	0.693	0.635	0.829	0.491	0.588	0.678	0.668
Al_2O_3	18.90	20.70	16.40	17.60	17.80	3.90	5.48	16.70	17.70	17.70	14.90	18.40	17.80	18.6	17.40
Fe_2O_3	3.85	11.50	7.38	8.26	7.41	8.47	13.81	5.01	4.89	4.48	4.99	3.84	3.61	4.42	3.82
FeO	3.00	—	4.70	4.98	5.30	5.88	7.64	4.94	4.10	5.87	4.50	3.89	3.24	3.76	4.40
MnO	0.13	0.13	0.21	0.18	0.24	0.15	0.18	0.14	0.29	0.06	0.16	0.08	0.15	0.13	0.14
MgO	4.43	6.49	6.54	6.69	7.22	13.40	11.20	6.13	4.82	4.39	6.18	3.59	2.79	3.03	3.96
CaO	13.60	15.40	13.20	15.30	14.90	20.00	16.70	7.39	9.01	6.11	8.81	6.78	7.02	6.69	5.68
Na_2O	3.56	1.22	1.91	1.04	1.03	0.20	0.35	2.70	2.54	3.93	3.61	3.68	3.70	4.02	5.73
K_2O	0.37	0.60	0.97	0.49	0.33	0.02	0.57	3.39	3.58	2.66	1.83	3.64	3.38	3.50	1.09
P_2O_5	0.46	0.08	0.36	0.42	0.15	0.02	0.04	0.27	0.25	0.27	0.29	0.25	0.37	0.25	0.28
H_2O^+	1.1	1.3	1.3	1.6	1.8	0.6	1.0	2.2	2.3	2.2	1.6	1.4	1.9	1.4	1.8
CO_2	0.02	0.01	0.17	0.03	0.02	0.02	0.11	0.19	0.36	0.14	0.65	0.28	2.24	0.03	0.17
SUM	99.79	100.18	97.86	99.51	99.04	98.76	98.73	97.98	99.23	98.44	98.85	98.12	99.09	99.01	99.64
LOI	1.35	1.10	1.35	1.55	1.60	0.40	0.55	1.95	2.70	2.20	2.25	1.75	4.25	1.48	1.75
D.I.	30.17	31.53	19.50	10.37	9.50	1.57	2.40	38.67	38.55	45.62	37.43	49.58	50.72	51.52	52.34
T_{Zr} (°C)	574.38	518.05	511.47	464.60	490.75	103.10	206.29	601.24	584.12	638.87	582.03	619.31	640.25	642.11	635.46
Trace Elements															
Ba[1]	263	333	442	251	315	88	254	2210	1670	899	589	1460	1390	1694	724
Rb[1]	17	10	23	16	9	5	22	64	53	53	26	64	29	64	27
Sr[1]	1180	1145	814	1060	988	84	136	487	562	704	544	537	742	563	587
Nb[1]	7	4	4	4	4	6	6	4	5	5	5	4	8	6	6
Zr[1]	69	28	39	14	25	23	28	51	50	65	72	50	72	71	64
Y[2]	14.74	—	—	14.14	—	6.90	—	—	—	—	—	10.74	16.96	18.22	—
Ni[1]	7	8	12	12	8	46	54	40	16	14	27	10	6	4	16
Cr[1]	b.d.	14	23	b.d.	22	182	52	99	37	55	133	29	26	13	49
V[2]	259.38	—	—	481.36	—	382.35	—	—	—	—	—	194.01	216.15	220.37	—
Sc	25.49[2]	39.3[3]	42.9[3]	48.06[2]	37.4[3]	121.80[2]	98.8[3]	40.3[3]	26.4[3]	21.4[3]	35.9[3]	15.42[2]	15.09[2]	16.94[2]	20.6[3]
Hf[2]	0.87	—	—	0.63	—	0.55	—	—	—	—	—	1.30	1.96	1.73	—
Ga[1]	28	28	29	30	29	23	25	24	27	25	26	29	30	28	27
Zn[1]	124	66	69	69	124	54	76	53	91	34	50	39	60	44	74
Cs[2]	1.42	—	—	1.02	—	0.02	—	—	—	—	—	0.72	0.10	0.32	—
Ta[2]	0.54	—	—	0.37	—	0.32	—	—	—	—	—	0.31	0.46	0.40	—

[1]XRF Pressed Pellet
[2]Induced Coupled Plasma Mass Spectrometry
[3]Neutron Activation
D.I. = qz + or + ab + ne + lc (normative mole %), TZ = Pothook/Hybrid Transitional Zone

recorded in the intrusive units (ave 0.54 wt%). Clinopyroxene from the Iron Mask batholith contains significant calculated Fe^{3+} (Fig. 5c), showing a total range of 0.02 to 0.19 cations per formula unit. The high Fe^{3+} contents of clinopyroxene from the Iron Mask batholith are consistent with crystallization under a relatively higher oxygen fugacity, as expected in alkaline magmas (e.g., LeBas, 1962). Additionally, island arc suites are characterized by high Fe^{3+} contents in clinopyroxenes implying systematically higher oxygen fugacities than other tectonic environments (Barsdell, 1988). Analyses of clinopyroxene collected from the transitional zone between the Pothook and Iron Mask hybrid unit contain consistently greater Fe^{3+} than clinopyroxene from uncontaminated Pothook rocks (Fig. 5c). This Fe^{3+} enrichment in pyroxenes from the Iron Mask hybrid unit, and particularly in the rocks from the transitional zone, suggests more highly oxidizing conditions during the assimilation/hybridization process.

Geochemistry

Major and Trace Elements

Whole rock major and trace element compositions of intrusive units and the Iron Mask hybrid unit are given in Table 3. Chemically, the Iron Mask batholith is alkaline to mildly subalkaline (Fig. 6a). Trace element compositions show the Iron Mask batholith to have volcanic arc affinities on tectonic discrimination diagrams (Fig. 6b).

Compositions of Pothook and Cherry Creek rocks show strong negative correlations between SiO_2 and CaO, MgO and FeO(T). Sugarloaf rocks have intermediate SiO_2 and do not follow this trend; they are relatively enriched in MgO and depleted in CaO for a given SiO_2. Iron Mask intrusive rocks have consistent Al_2O_3 (14.9 - 19.4 wt%) over the entire range of SiO_2. Widespread K-feldspar metasomatism of Pothook and Cherry Creek rocks and abundant titanite in some samples from the Cherry Creek make it difficult to evaluate intersuite variation in TiO_2 and K_2O. However, Sugarloaf rocks are highly enriched in K_2O and marginally depleted in TiO_2 (and Na_2O) compared with other Iron Mask intrusive rock compositions.

Chemical analyses of rocks from the Iron Mask hybrid unit show significant variation in only a few of the major elements. Samples IM-173 and IM-306 represent the matrix of Type I and Type II hybrid. There are two analyses of Type III matrix (IM-120, IM-256) and two analyses of recrystallized (pyroxenite) xenoliths. One xenolithic sample (IM-121) is part of a 0.2 m diameter fragment found just inside the margin of the batholith whereas the other (IM-268) is from a 250 m clast near the Ajax pits. Rocks from the Iron Mask hybrid unit are more basic (40.5 - 43.7 wt% SiO_2), depleted in alkalis and enriched in TiO_2 and CaO compared to the intrusive rocks in the batholith. They are highly variable in Al_2O_3, MnO and P_2O_5. Analyses of the two xenoliths are similar in major element concentrations to a sample from a pyroxene-phyric andesitic flow of the Nicola Group near the western margin of the batholith (IM-185).

Based on measured FeO and Fe_2O_3, most Pothook and Iron Mask dike rocks are Ol + Ne-normative. One Pothook sample (IM-119) is Hy-normative and one dike (IM-254) contains quartz in the norm. Cherry Creek rocks are mainly Qz-normative with only one sample (IM-237) containing calculated olivine and nepheline. Most rocks from the Sugarloaf unit are Ol + Hy-normative, however, one sample is Qz + Co-normative (IM-266) and another contains normative nepheline (IM-271). Iron Mask hybrid units are either Hy or Ne-normative. Because samples collected from the Iron Mask batholith can be altered or show the effects of deep weathering, the measured Fe_2O_3 may not reflect magmatic conditions. Norms were also calculated with $Fe_2O_3 = 0.15\ Fe_T$ for comparison. The results are that only 3 samples are Qz-normative and nepheline dominates. None of the purely magmatic rocks showed normative leucite.

Trace element abundances for rocks of the Iron Mask batholith (Table 3) show significant overlap in all units; only a few differences are observed. Sugarloaf rocks are slightly enriched in Cr and Ni and depleted in Sr, in comparison with Pothook and Cherry Creek samples. The compositions of Type II and Type III Iron Mask hybrid are relatively depleted in Ba and Rb compared to the intrusive phases.

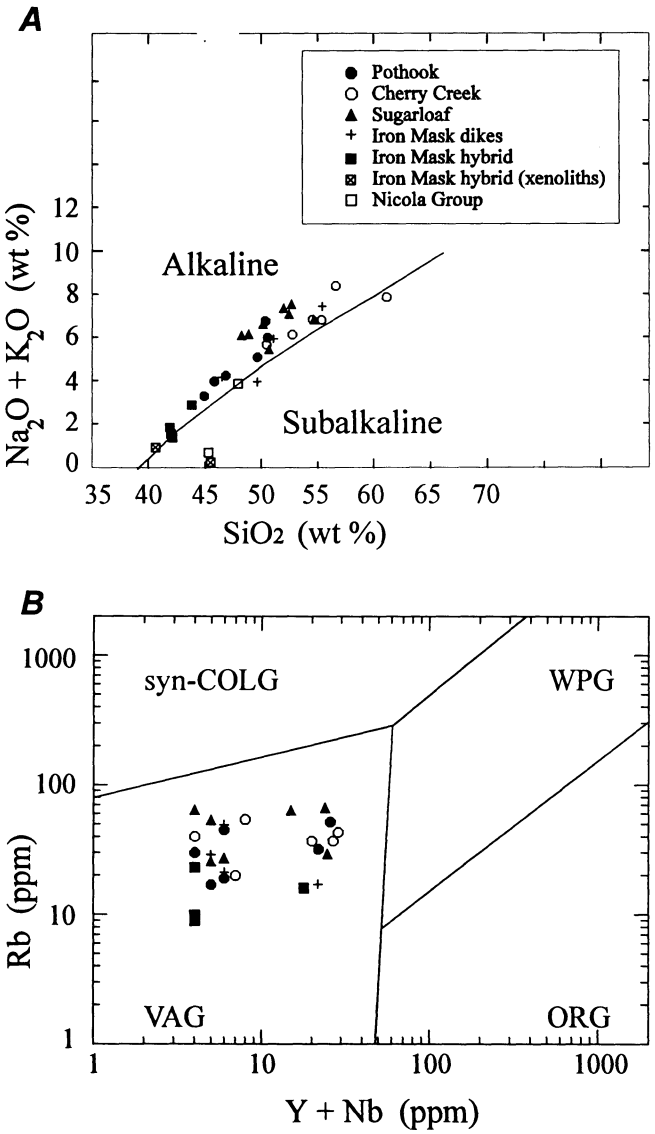

FIGURE 6. Iron Mask hybrid and Nicola Group rocks plotted as: (A) SiO_2 vs $Na_2O + K_2O$ (Irvine and Baragar, 1971), and (B) Rb vs Y + Nb) which separates volcanic arc (VAG), syn-collision, within-plate (WPG) and ocean ridge (ORG) granites (Pearce et al., 1984).

Zircon Saturation Index

Rocks from the Iron Mask batholith contain very little Zr (14-86 ppm) and almost no modal zircon (Mortensen et al., this volume), suggesting that zircon should crystallize relatively late or perhaps not occur at all. The saturation potential of zircon can be modeled as a function of bulk rock chemistry using the model of Watson and Harrison (1983, 1984). They provide an empirical model for predicting the hypothetical zircon saturation temperature (T_{Zr}) for a specific zircon concentration and rock composition. The equation is:

$$D^{zir/liq}_{Zr} = \{-3.8 - [0.85(M - 1)]\} + 12900/T \quad \ldots\ldots\ldots\ldots\ldots (1)$$

where M is the cation ratio (Na + K + 2Ca)/(Si • Al) and T the

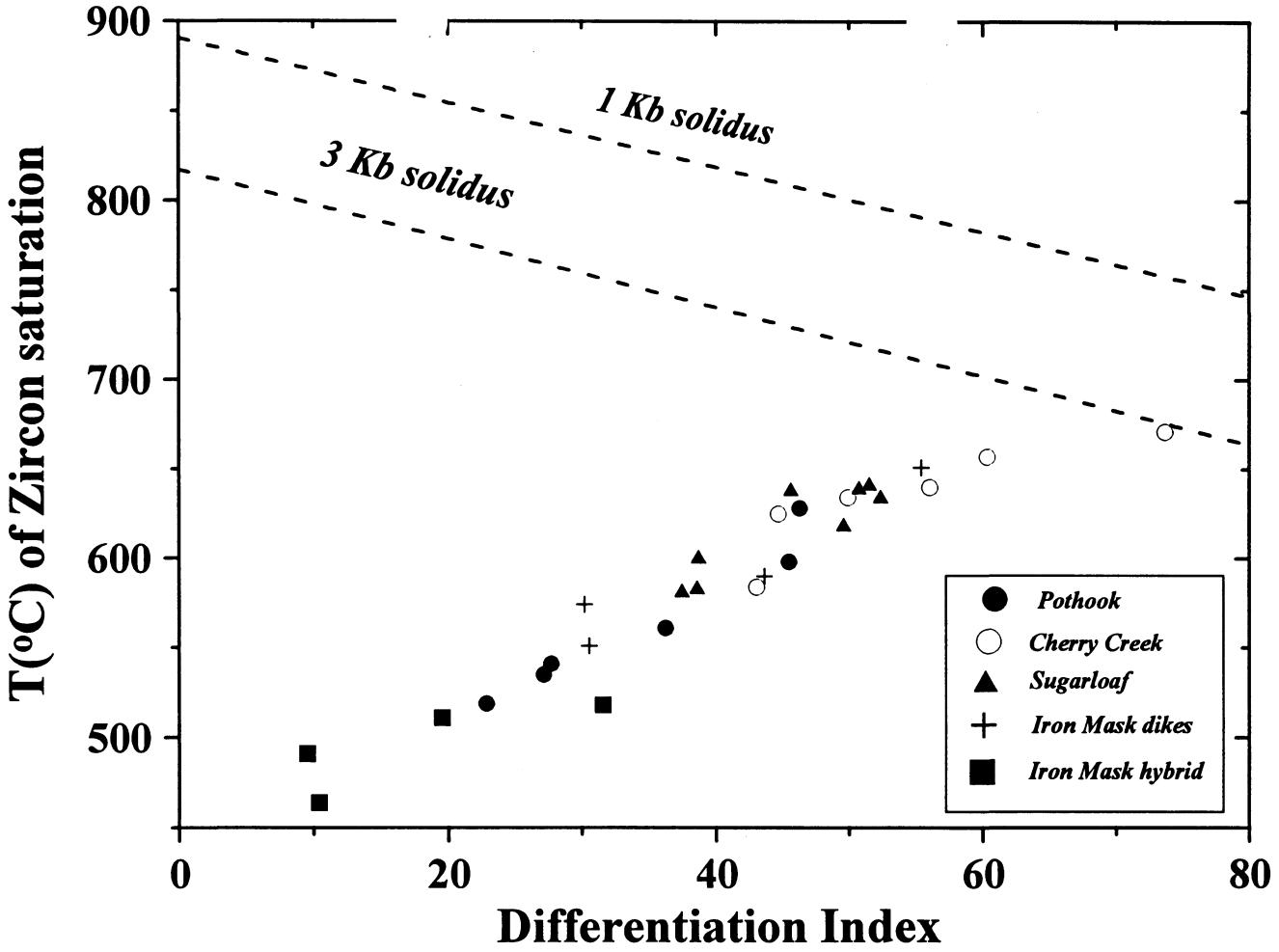

FIGURE 7. Computed zircon saturation temperatures (T_{Zr}°C) for Iron Mask rocks are plotted against D.I. (sum of normative qz + ab + or + ne + lc). Highest D.I. values are associated with most felsic rocks which also record the highest T_{Zr} indicating the greatest potential for zircon saturation (see text).

absolute temperature. High T_{Zr} implies that the rock may crystallize zircon as an early igneous phase while low T_{Zr} suggests that the rock will only saturate with respect to zircon toward the end of crystallization (near solidus). The calculated zircon saturation temperatures (T_{Zr}) for rocks of the Iron Mask batholith range from 464°C to 670°C (Table 3).

Figure 7 plots calculated T_{Zr} against the Differentiation Index (D.I.) for rocks in the Iron Mask batholith (xenoliths in the Iron Mask hybrid are excluded). D.I. is the sum of normative quartz, albite, orthoclase, nepheline, leucite and kalsitite (Thornton and Tuttle, 1960) and is an estimate of relative differentiation. D.I.s for Iron Mask rocks range from 9.5 to 73.7, with the Iron Mask hybrid showing the least evolved signatures and Cherry Creek the most evolved.

Rocks of the Iron Mask batholith show a regular increase in D.I. with increasing T_{Zr}, consistent with the rocks representing an alkaline series of magmas which did not saturate with respect to zircon (Fig. 7). If zircon were to saturate, the calculated T_{Zr} would remain constant or decrease due to loss of Zr from the melt. Also shown in Figure 7 are surfaces representing the experimental magmatic solidus for water-saturated melts at 1 Kb and 3 Kb. Rock compositions and Zr concentrations of Iron Mask hybrid rocks suggest that zircon is well below saturation throughout crystallization. Pothook rocks exhibit the most variation in D.I. and a range of T_{Zr} from 519°C to 628°C. These data suggest that zircon would not saturate in Pothook magma (cf, solidus curves). Sugarloaf rocks are slightly more differentiated than Pothook rocks, but T_{Zr} (582°C to 642°C) is still sufficiently low to inhibit early crystallization of zircon. Cherry Creek rocks have the highest D.I. and the highest T_{Zr} (585°C to 671°C). These rocks represent the best candidates in the Iron Mask batholith for containing early magmatic zircon. The trend established for Cherry Creek rock compositions flattens at the most evolved sample, suggesting that zircon may have saturated.

Results of this modeling imply that for alkaline magmas having low Zr concentrations, such as the Iron Mask rocks, zircon crystallization is restricted to the last stages. To date, the only successful U-Pb dates from Iron Mask rocks are from the Cherry Creek (205 ± 4 Ma) and from a coarse-grained Type III Iron Mask hybrid sample (204.6 ± 2.6 Ma). The Iron Mask hybrid zircons show strong inheritance (Mortensen et al., this volume) which suggests that the zircon recovered need not be indicative of primary magmatic crystallization. A reliable date has yet to be produced for the Pothook phase and zircon has not been recovered from any rocks belonging to the Sugarloaf phase (Mortensen et al., this volume).

Rare Earth Elements

The REE_{CN} profiles for all three intrusive rock units are similar in relative element abundance and shape (Fig. 8a). The patterns are slightly LREE enriched and flatten considerably toward the HREEs. $(La/Lu)_{CN}$ ratios are 3.42, 3.54 and 3.29 for the Pothook, Cherry Creek and Sugarloaf phases, respectively, and no Eu anomaly is apparent. The overlaps in enrichment and pattern attest to the consanguinity of these intrusive rocks. The only exceptions are a single dike which shows a small negative europium anomaly, consistent with minor plagioclase fractionation, and a sample of Sugarloaf which shows slightly lower REE_{CN} abundances but a similar overall pattern.

Profiles of the Iron Mask hybrid unit are decidedly different

TABLE 4. Summary of dist ishing features of intrusive phases of Mask batholith

	Pothook suite	Cherry Creek suite	Sugarloaf suite	Iron Mask hybrid unit
Field and petrographic features	weak to strong foliation late poikilitic biotite magnetite veining abundant early apatite cpx as primary mafic mineral abundant opaques in cpx An_{43}-An_{52}	tabular, interlocking or sub-trachytic feldspar weakly to strongly zoned plagioclase cpx, hbl or biotite as primary mafic phase sparce primary quartz An_{32}-An_{45}	hbl phenocrysts sparce cpx; no biotite trachytic texture in both hbl and feldspar An_{32}-An_{38}	abundant partially digested heterolithic xenoliths extreme textural and mineralogical variability abundant coarse magnetite pyroxene as dominant mafic mineral An_{60}
Intrusive relationships	gradational and intrusive contacts with the Cherry Creek unit transitional zone (50-250 m) between the Pothhook and Iron Mask hybrid	gradational to and brecciates the Pothook unit matrix of intrusive breccia with Iron Mask hybrid and Nicola Group clasts	intrudes all other units dikes and small stocks along the western margin of the batholith found as small dikes in Nicola Group volcanic rocks	gradational contact with Pothook suite and Nicola Group volcanic rocks gradational contacts between the three recognized types
Chemical Composition	monzonite-monzodiorite	gabbro-diorite	diorite	REE profiles parallel Nicola Group patterns
Mineralization/ Alteration	hosts lode magnetite-apatite deposits intense Kfs overprint at contacts with the Cherry Creek	intense Kfs alteration at Pothook diorite contacts hosts mineralization at the Crescent pit local secondary titanite	hosts mineralization at the Ajax property albitization is dominant alteration	local Kfs alteration

(Fig. 8b). Patterns for, Type III Iron Mask hybrid and the xenolith are similarly depleted in both the LREEs and the HREEs and relatively enriched in the MREEs. The profile of the xenolith has lower total REE abundances than the hybrid rock. The similarity in REE_{CN} patterns for a Nicola Group clinopyroxene-phyric andesitic flow (IM-185) and the recrystallized hybrid xenolith, strongly supports Nicola Group as the source of many of the xenoliths in the hybrid unit. Furthermore, REE_{CN} patterns for Type III Iron Mask hybrid lie between the patterns established for Pothook magma and Nicola Group rocks (and the recrystallized xenolith). These chemical relationships strongly support the idea that the hybrid itself derives from assimilation involving a Pothook-like magma and Nicola Group metavolcanic rocks.

Discussion And Conclusions

Magmatic Lineages

Table 4 presents a synopsis of characteristics for the rock units in the Iron Mask batholith. The textural and mineralogical similarities and locally gradational nature of the Pothook and Cherry Creek units suggest that these rocks may be derived from the same parental magma. This is supported by the continuous linear trends observed in most of the major elements when plotted against SiO_2. The Cherry Creek and Pothook suites differ, however, in: (1) plagioclase composition, (2) morphology and abundance of magnetite, (3) abundance of apatite, (4) morphology of biotite, (5) abundance of opaque inclusions in clinopyroxene and, (5) presence of primary quartz, amphibole and K-feldspar. Many of these differences could result from magmatic differentiation under changing physical conditions.

Sugarloaf rocks differ from the Pothook and Cherry Creek phases in occurrence, mineralogy, texture and chemistry. The Sugarloaf diorite definitely cross-cuts Pothook and Hybrid rocks. Amphibole is generally abundant and, in company with plagioclase,

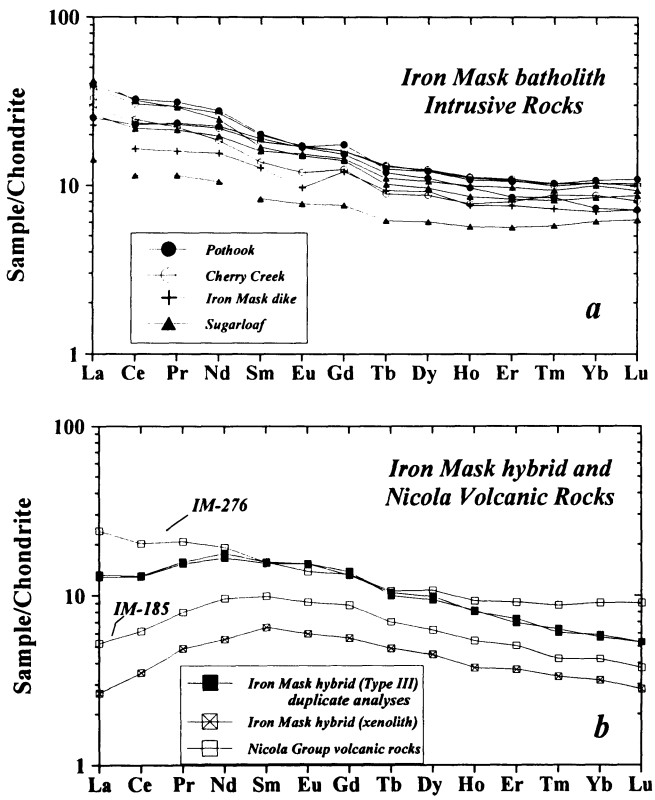

FIGURE 8. Chondrite normalized rare earth element (REE_{CN}) plots for: (A) magmatic rocks of the Iron Mask batholith, and (B) Iron Mask hybrid and Nicola Group rocks. Normalizing data derive from Boynton (1984).

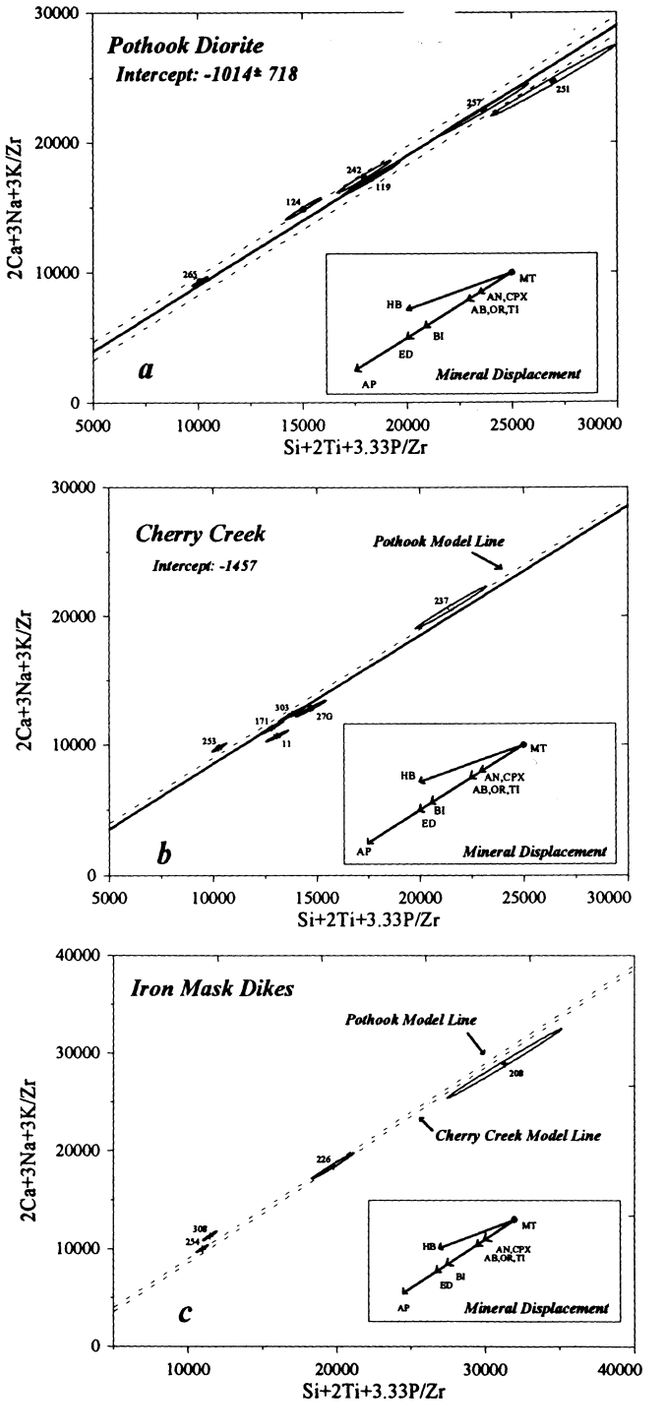

FIGURE 9. Pearce element ratio plots of [2Ca+3K+3Na/Zr] vs [Si+2Ti+3.33P/Zr] for different phases of the Iron Mask batholith, including: (A) Pothook diorite, (B) Cherry Creek monzodiorite to monzonite, and (C) late Iron Mask dikes. These Pearce element ratio plots model the compositional effects derived by sorting minerals Pl ± Cpx ± Kfs ± Ttn ± Bt ± Ap and the edenite component of amphibole solid solutions.

is commonly found as aligned phenocrysts in a very fine-grained groundmass, suggesting a hypabyssal environment of emplacement. Clinopyroxene in Sugarloaf rocks is less abundant and is chemically and optically distinct from clinopyroxene in the Pothook and Cherry Creek units (Fig. 5). Sugarloaf rocks do not necessarily fall on the major element compositional defined by the Cherry Creek and Pothook units. Finally, the alteration style of Sugarloaf diorite is dominated by albitic alteration as opposed to the K-feldspar and epidote assemblage of the other intrusive phases. Consequently, despite the similarities in REE_{CN} composition, the Sugarloaf intrusive suite may represent a rate and younger magmatic event within the Iron Mask batholith.

The process of testing genetic linkages concerning the intrusive phases of the Iron Mask batholith was undertaken using Pearce element ratio diagrams (Pearce, 1968; Russell and Nicholls, 1988; Nicholls and Russell, 1991). Diagrams (cf, Fig. 9) are designed by: (1) choosing an appropriate conserved element for the denominator, and (2) choosing a set of numerator elements for the X- and Y-axes that will model the effects of the target mineral assemblage (Stanley and Russell, 1989). The low calculated zircon saturation temperature (T_{Zr}) of rocks from the Iron Mask batholith suggests that Zr was retained in the melt phase throughout much of the crystallization history. Therefore, Zr is potentially a conserved element in these rocks and was chosen as the denominator element.

The axes that are used in Figure 9 model the fractionation of feldspar, clinopyroxene, biotite, apatite, titanite and the edenite component of amphibole as a slope of 1. Magnetite and quartz fractionation have no effect on the diagram, and common hornblende causes displacements less than one. Error ellipses on each data point are shown for 1σ analytical error as determined through duplicate analyses (Snyder, 1994).

Compositional variations in the Pothook unit are shown in Figure 9a. The model line was constructed by averaging lines representing a slope of one through each data point and is shown with 1σ error (dashed lines). Fractionation of the observed mineral assemblage in the Pothook rocks (plagioclase, clinopyroxene, biotite, K-feldspar, apatite and titanite) accounts for the variation among three of the samples. Three compositions do not fall on the model line, but two (IM-242 and IM-124) lie within the uncertainty envelope calculated for the model trend. These samples derive from near the transitional zone with the Iron Mask hybrid and it is possible that their compositions are slightly modified by hybridization or alteration of Pothook magma. Sample IM-251 is statistically off the model trend and was collected very close to the Cherry Creek contact. It may, in fact, have a stronger Cherry Creek affinity than was recognized or be affected by processes other than fractionation (e.g., mixing or metsomatism).

Cherry Creek compositions are shown on the same type of diagram in Figure 9b. The dashed line is the model fractionation trend fitted to the Pothook rocks (Fig. 9a) and the heavy solid line represents a reference line for Cherry Creek rocks. It was drawn through IM-303, a sample from the southern end of the batholith. Cherry Creek rocks, as a group, neither fit the Pothook fractionation trend nor define a single trend of their own. Samples IM-237 and IM-253 lie very close to the Pothook model line, suggesting that they may be genetically related to the Pothook through fractionation. Samples IM-303, IM-171, and IM-27G are consistent with a single model trend (e.g., unit slope), which implies that they could belong to a single magma batch. Sample IM-11, however, appears to be inconsistent with fractionation of the modal mineral assemblage. Figure 9b implies: (1) not all Cherry Creek rocks can be related by fractionation of the model assemblage to a single magma batch, (2) some Cherry Creek rocks show a chemical affinity to the Pothook suite, and (3) compositional trends established for Pothook and Cherry Creek rocks are so similar (cf. intercepts to model lines) as to be indistinguishable.

Compositions of late dikes found throughout the Iron Mask batholith are compared against the trends established for Pothook and Cherry Creek rocks in Figure 9c. The dikes are both mineralogically and chemically diverse, however, all of the dikes fall within a 'compositional envelope' defined by rock compositions of the Pothook and Cherry Creek units. The fact that the intercepts to the Pothook and Cherry Creek model lines cannot be distinguished suggests that the two suites derive from the same or chemically indistinguishable magmatic systems. The fact that the compositions of these dikes fall on the same trends, implies that they too derive from the same system(s).

Compositions of Sugarloaf rocks are plotted on the same type of element ratio diagram in Figure 10. A reference model line with

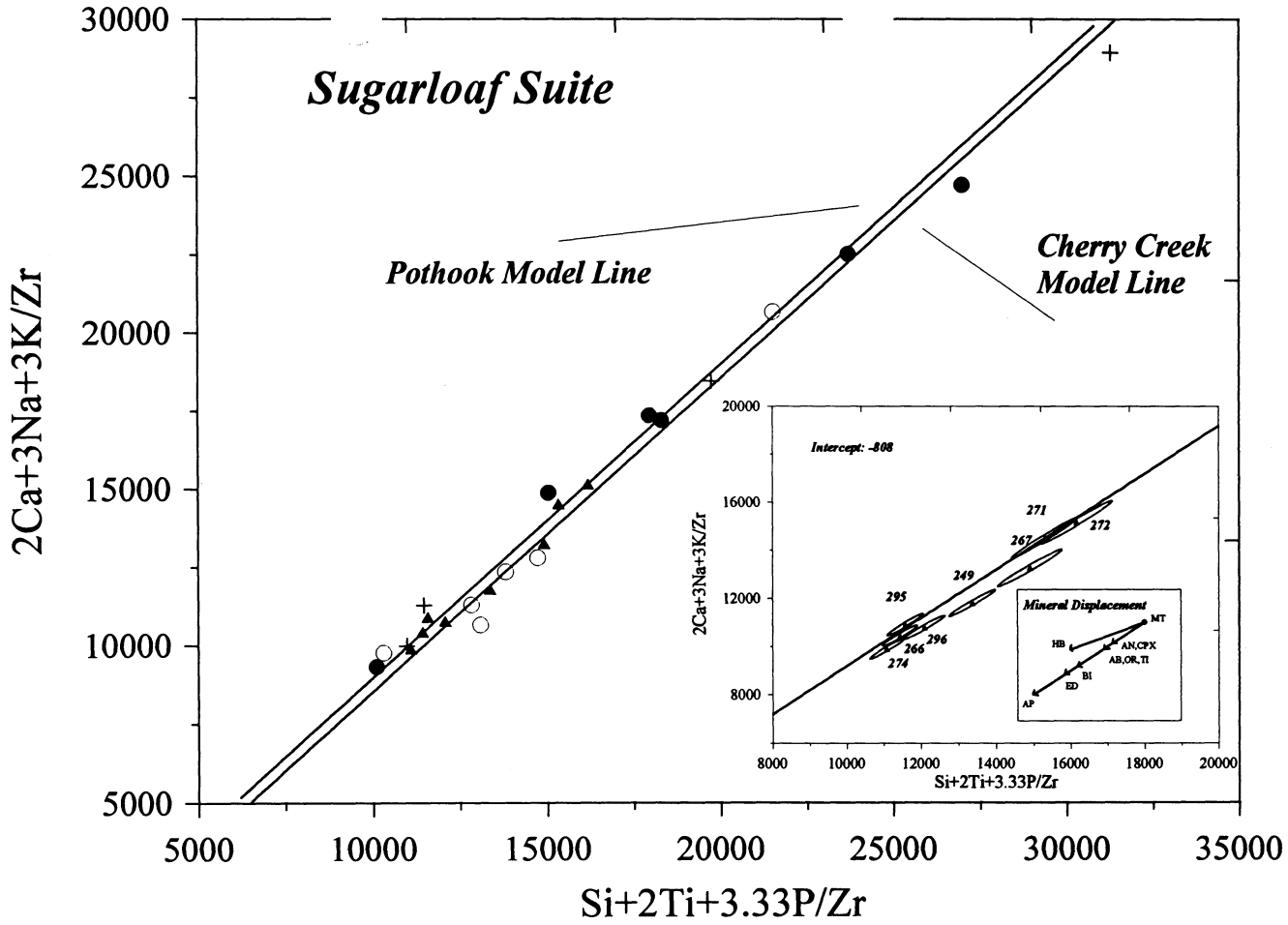

FIGURE 10. Pearce element ratio plot showing distribution of Sugarloaf suite rocks (triangles) compared to compositions of Pothook, Cherry Creek and late dike rocks (symbols as in Fig. 9). Also shown are trends established for Pothook and Cherry Creek rocks and enlarged view (inset) of Sugarloaf data set.

unit slope is drawn through a sample taken from the type locality on Sugarloaf Hill (Fig. 10, inset). The suite as a whole does not define a single magmatic trend in this space, indicating that either the Sugarloaf suite comprises more than one magma batch or differentiation involved phases other than plagioclase, edenitic-amphibole, clinopyroxene, biotite, K-feldspar, apatite and titanite. These rocks also span a narrower compositional range than the other intrusive units, although the Sugarloaf rocks do straddle the model trends established for the Pothook and Cherry Creek suites (Fig. 10). The latter point is an important one as the Sugarloaf rocks do not span these trends by chance. The distribution of Sugarloaf compositions shows that these rocks have a definite chemical affinity to the rest of the Iron Mask batholith, although they do not represent a single magmatic system.

Origins of the Iron Mask Hybrid

The Iron Mask hybrid unit was first treated as a separate mappable unit with an origin different from that of the Pothook, Cherry Creek and Sugarloaf intrusions by Preto (1972) and Northcote (1977). Snyder and Russell (1993) mapped and sampled a transitional zone between Pothook diorite and Type II Iron Mask hybrid unit, which provides insight into the nature of the 'hybridization' process. Uncontaminated Pothook diorite can be traced into a gradational zone of hybridized rocks, which clearly shows interaction between Pothook magma and Nicola Group country rocks. Clasts derived from the Nicola Group are rounded, recrystallized and partially digested suggesting mass transfer between these two end-member systems. Indeed, some exposures freeze this process in place, with pieces of recrystallized xenoliths being physically disaggregated and the crystals being incorporated into the magmatic phase (Fig. 3c, lower).

Partial incorporation of xenolithic material is defined as *selective assimilation* as opposed to total fusion or *bulk assimilation*. The "mixing line" between the two end-member compositions that are involved in selective assimilation need not be linear. This is because, firstly, the xenolith variety and abundance is not uniform between outcrops and, secondly, because not all of the xenolithic material is necessarily assimilated. The hybridization/assimilation process is selective and incorporates constituents which are the most mobile under magmatic conditions. Thirdly, it is likely that different parts of the 'hybridization system' were operating under different physical and chemical conditions. For example, variations in the depth (pressure), temperature, the ratio of magma to xenolith, and the type and amount of xenolithic material available could account for many of the differences manifest in the varieties of Iron Mask hybrid: namely, xenolithic (Types I and II) and non-xenolithic (Type III).

Type III Iron Mask hybrid probably represents the effects of more complete fusion and assimilation of Nicola Group rocks, and as such, provides the best opportunity to evaluate the relative chemical contributions of the two end-members. Major and trace element chemistry do not appear to define a linear mixing line, although compositional data on different rock types within the Nicola Group are sparse. REE_{CN} patterns of Nicola Group and Iron Mask hybrid rocks, however, elucidate one aspect of the assimilation and hybridization process. The Type III Iron Mask hybrid has a similar but relatively enriched REE_{CN} pattern (Fig. 8b) compared to Nicola Group volcanic rocks and shows a relatively depleted

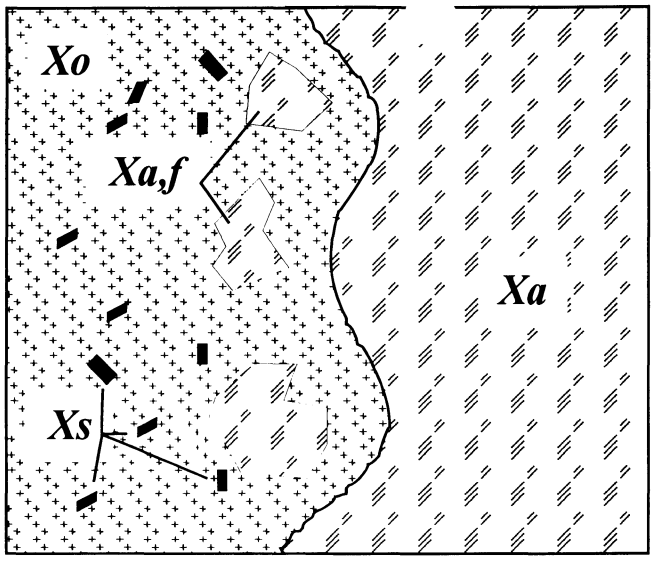

FIGURE 11. Schematic representation of the steps and variables needing definition to model evolution of volatile constituents during magmatic assimilation of Nicola Group rocks by Pothook magma. Major variables include the mole fraction of H_2O in: the original magma (X_o), the country rock being assimilated (X_a), the crystallization assemblage (X_s), and in the recrystallized and hybridized xenoliths ($X_{a,f}$).

REE_{CN} pattern compared to Pothook rocks. The REE_{CN} data are permissive of the idea that chemical and physical mixing of Pothook magma and Nicola Group rocks produced the "hybrid" rock unit.

One consequence of recrystallization and partial assimilation of Nicola Group rocks by Pothook magma is a change in the volatile budget of the system. Russell and Snyder (1993a, 1993b) have identified a number of variables which contribute to the volatile content of a system being affected by magmatic assimilation. A schematic representation of the selective assimilation process and the components described above is shown in Figure 11. The variables include: the original water content of the magma (X^o), the water incorporated into the crystallizing assemblage (X_s), the original water content of the assimilated material ($X_{a,o}$), the final water content of the residual xenoliths ($X_{a,f}$), the ratio of crystallization to assimilation (α), and the amount of material that is added to the system through partial fusion of the assimilant (r). These parameters may be used in the equation:

$$x_r = \frac{[x^o - x_s F + (x_{a,o} - x_{a,f})] \bullet \alpha F}{[1 - F + r\,\alpha\,F]} \quad \ldots\ldots\ldots\ldots\ldots\ldots (2)$$

to model the volatile production induced by selective assimilation as a function of crystallization. The variable F is the fraction of original magma crystallized and ranges from 0 to 1, where 1 represents complete crystallization.

Table 5 lists values pertinent to the Iron Mask situation. These parameters are estimated from field and petrographic observations as well as from chemical analyses. Textural relationships in the Pothook diorite between plagioclase and clinopyroxene and the absence of primary amphibole suggests a water-undersaturated initial melt composition (X^o) (Eggler, 1972; Naney, 1983). The amount of water in the Nicola group volcanic rocks before and after recrystallization (X_a and X_f, respectively) are derived from chemical analyses of these rock types. The water in the crystallizing assemblage (X_s) is estimated from the modal mineralogy of Pothook and Cherry Creek rocks and the amount of material incorporated into the Pothook magma (r) is estimated from field observation.

Figure 12a shows the results of selective assimilation of Nicola Group rocks into the Pothook diorite constructed from values in Table 5. The model paths are shown as F (fraction of magma crystallized) vs the water content (mole%) of the system and map model lines for several ratios of assimilation to crystallization (α). Also shown is the model line for crystallization of Pothook diorite with no assimilation and a crystallizing assemblage with 0.2 mole% average water content (X_s) as well as a model line calculated with r = 0.5, which represents more complete assimilation. In addition, the 2 Kb and 4 Kb saturation surfaces are represented. The intersections between these surfaces and the model volatile production paths define, for a given confining pressure, the point (F) at which we expect initiation and possible separation of a volatile phase.

TABLE 5. Values of ‹ ›tants used to model volatile production in Iron Mask batholith

Model	X^o	X_s	X_a	X_f	α	r
Crystallization	0.085	0.0-0.08	—	—	—	—
Bulk Assimilation and Crystallization	0.085	0.02	0.075	—	0.2-5	—
Selective Assimilation and Crystallization	0.085	0.02	0.075	0.02	—	0.15
Selective Assimilation (Dehydration)	0.085	0.02	0.075	0.02	—	0.075

Figure 12a suggests that, for all values of α, selective assimilation of Nicola Group rocks by Pothook magma may potentially raise the volatile content of the magma, thus promoting exsolution of a volatile phase earlier in the crystallization history. For example, with no assimilation at a confining pressure of 2 Kb, the Pothook system may saturate with water at 58% crystallization while during selective assimilation with r = 0.15 and α = 1, it may saturate at only 44% crystallization. For Pothook magmas, the higher the ratio of crystallization to assimilation is, the greater the degree of volatile enrichment. Most significantly, it is shown that the value of r (material added to the system) has a very large effect on the volatile budget. When a large amount of material is added to the magmatic system (r = 0.5), the process serves to inhibit volatile production.

Figure 12b illustrates the consequences of one end-member style of selective assimilation: thermal dehydration of the xenolithic material, without the incorporation of non-volatile components. In other words, this model assumes that no material is added to the magmatic system except for the volatiles stored in the assimilant. As expected, this process enhances volatile production to an even greater degree. This can be seen by comparing the curves computed for the two models using α = 1 (cf. Fig. 12b). The dehydration assimilation model promotes volatile exsolution as early as 42% crystallization at 2 Kb confining pressure; the concept is probably especially applicable to the margins of the magmatic system.

Results of modeling selective assimilation in the Iron Mask batholith indicate that the recrystallization of hydrous material (greenschist Nicola volcanic rocks) to a more anhydrous assemblage (the 'pyroxenite' xenoliths of the Iron Mask hybrid unit) has the potential for raising the volatile content of a magma (Pothook). The most influential parameter in this process is the amount of material incorporated into the melt phase. If a large amount of material is added (as in wholesale assimilation), the dilution effects of the additional material offset the total volatiles in the system. If, instead, selective dehydration reactions are considered, then the volatile content of the magmatic phase is increased dramatically. The water content of a magma is of interest because it affects the density and viscosity of the magma and the potential for exsolving a volatile phase. A magma that has a higher volatile content will exsolve a fluid phase earlier in its crystallization history. Magmatic fluid phases can play a significant role in developing and sustaining hydrothermal activity, thus assimilation-induced volatile production ultimately can play a significant role in the formation of magmatic-hydrothermal ore deposits.

Acknowledgments

This research comprises a major portion of the senior author's M.Sc. thesis research during her tenure at The University of Brit-

ish Columbia. The research was supported by diverse funding accrued by the Mineral Deposit Research Unit at The University of British Columbia in support of the Copper-Gold Porphyry Deposits Research Program. Amongst the sources of funding are the Natural Sciences and Engineering Research Council of Canada, the Science Council of British Columbia and the following industry sponsors: BP Resources Canada Ltd., Homestake Canada Inc., Kennecott Canada Inc., Placer Dome Ltd., Princeton Mining Corporation, Rio Algom Exploration Inc., and Teck Corporation. We are indebted to a number of people for stimulating discussion and occasional direction, most notably Drs. J.F.H. Thompson, C.I. Godwin, C.R. Stanley and J.R. Lang. Arne Toma kindly lent technical support at various stages of the research. The manuscript was improved significantly through the review process, chiefly by the efforts of Darryl Drummond and Vic Preto and the editorial work of Tom Schroeter. The authors accept full responsibility, however, for any remaining aberrations or inconsistencies. This paper represents MDRU publication number 53.

REFERENCES

BARTON, M. and VAN BERGEN, M.J., 1981. Green clinopyroxenes and associated phases in a potassium-rich lava from the Leucite Hills, Wyoming. Contributions to Mineralogy and Petrology, 77, p. 101-114.

BARSDELL, M., 1988. Petrology and petrogenesis of clinopyroxene-rich tholeiitic lavas, Merelava Volcano, Vanuatu. Journal of Petrology, 29, p. 927-964.

BEDARD, J.H.J., FRANCIS, D.M. and LUDDEN, J., 1988. Petrology and pyroxene chemistry of Monteregian dykes: The origin of concentric zoning and green cores in clinopyroxenes from alkali basalts and lamprophyres. Canadian Journal of Earth Sciences, 25, p. 2041-2058.

BOYNTON, W.V., 1984. Cosmochemistry of the Rare Earth Elements: Meteorite studies. *In* Rare Earth Geochemistry. *Edited by* P. Henderson. Elsevier, Amsterdam, p. 63-114.

BROOKS, C.K. and PRINTZLAU, I., 1978. Magma mixing in mafic alkaline volcanic rocks: The evidence from relict phenocryst phases and other inclusions. Journal of Volcanology and Geothermal Research, 4, p. 315-331.

CANN, R.M., 1979. Geochemistry of magnetite and the genesis of magnetite-apatite lodes in the Iron Mask Batholith, B.C. Unpublished M.Sc. thesis, The University of British Columbia, Vancouver, British Columbia, 196 p.

CARR, J.M., 1956. Copper deposits associated with the eastern part of the Iron Mask Batholith near Kamloops. *In* British Columbia Minister of Mines, Annual Report, 1956, p. 47-69.

CARR, J.M. and REED, A.J., 1976. Afton: A supergene copper deposit. *In* Porphyry Deposits of the Canadian Cordillera. *Edited by* A. Sutherland Brown. Canadian Institute of Mining and Metallurgy, Special Volume 15, p. 376-387.

COCKFIELD, W.E., 1948. Geology and Mineral Deposits of Nicola Map Area, British Columbia. Geological Survey of Canada, Memoir 249.

CUNDARI, A. and SALVIULO, G., 1989. Ti solubility in diopsidic pyroxene from a suite of New South Wales leucitites (Australia). Lithos, 22, p. 191-198.

EGGLER, D.H., 1972. Water-saturated and undersaturated melting relations in a Paricutin andesite and estimate of water content in the natural magma. Contributions to Mineralogy and Petrology, 34, p. 261-271.

EWING, T.E., 1981a. Regional stratigraphy and structural setting of the Kamloops Group, south-central British Columbia. Canadian Journal of Earth Sciences, 18, p. 1464-1477.

EWING, T.E., 1981b. Petrology and geochemistry of the Kamloops Group volcanics, British Columbia. Canadian Journal of Earth Sciences, 18, p. 1478-1491.

EWING, T.E., 1982. Geology of the Kamloops Group near Kamloops. British Columbia Ministry of Energy, Mines and Petroleum Resources, Preliminary Map No. 48 and accompanying notes, 19 p.

HOILES, H.H.K., 1978. Nature and Genesis of the Afton Copper Deposit, Kamloops, British Columbia. Unpublished M.Sc. thesis, The University of Alberta, Edmonton, Alberta.

IRVINE, T.N. and BARAGAR, W.R.A., 1971. A guide to the chemical classification of the common volcanic rocks. Canadian Journal of Earth Sciences, 8, p. 523-548.

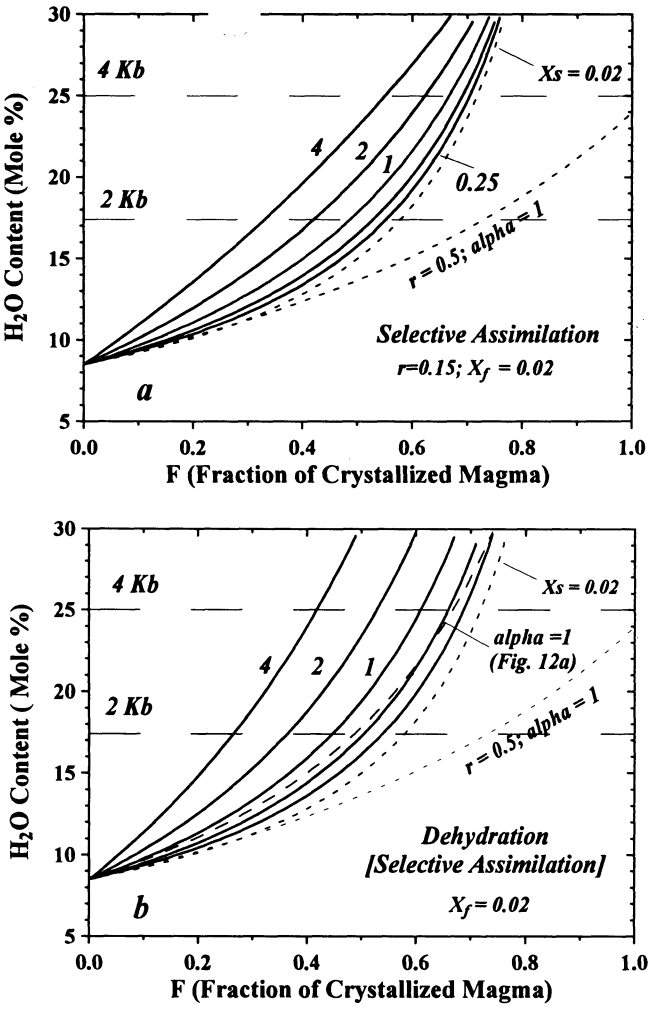

FIGURE 12. Summary of calculated model assimilation paths presented as predicted H_2O concentration in the derived magma as a function of crystallization. Paths are shown for different ratios of crystallization to assimilation ($\alpha = 0.25, 0.5, 1, 2, 4$). Figure 12A shows the consequences of coupled crystallization and selective assimilation with an r value of 0.15; whereas Figure 12B summarizes the paths calculated for dehydration-style selective assimilation (solid curves); the dashed line for $\alpha = 1$ serves as a comparison to the paths shown in Fig. 12a.

KWONG, Y.T.J., 1987. Evolution of the Iron Mask Batholith and its associated copper mineralization. British Columbia Ministry of Energy, Mines and Petroleum Resources, Bulletin 77, 55 p.

LANG, J.R., 1994. Geology of the Crescent alkalic porphyry copper-gold deposit, Afton mining camp, British Columbia (92I/9). *In* Geological Fieldwork 1993. *Edited by* B. Grant and J.M. Newell. British Columbia Ministry of Energy, Mines and Petroleum Resources, Paper 1994-1, p. 285-296.

LANG, J.R. and STANLEY, C.R., 1995. Contrasting styles of alkalic porphyry copper-gold deposits in the northern Iron Mask Batholith, Kamloops, British Columbia. *In* Porphyry Deposits of the Northwestern Cordillera of North America. *Edited by* T.G. Schroeter. Canadian Institute of Mining, Metallurgy and Petroleum, Special Volume 46.

LEBAS, M.J., 1962. The role of aluminum in igneous clinopyroxenes with relation to their parentage. American Journal of Science, 260, p. 267-288.

MATHEWS, H.M., 1941. Geology of the Iron Mask Batholith. Unpublished M.Sc. thesis, The University of British Columbia, Vancouver, British Columbia, 42 p.

MEHNERT, K.R., 1971. Migmatites and the Origin of Granitic Rocks. Elsevier Publishing Company, 405 p.

MONGER, J.W.H., 1989a. Overview of Cordilleran Geology. *In* Western Canada Sedimentary Basin: A Case History. *Edited by* B.D. Ricketts. Canadian Society of Petroleum Geologists, Institute of Sedimentary and Petroleum Geology, p. 9-32.

MONGER, J.W.H., 1989b. Geology of tl pe and Ashcroft Map Areas, British Columbia. Geological Surve, of Canada, Maps 41-1989 and 42-1989.

MONGER, J.W.H., PRICE, R.A. and TEMPELMAN-KLUIT, D.J., 1982. Tectonic accretion and the origin of two major metamorphic and plutonic welts in the Canadian Cordillera. Geology, 10, p. 70-75.

MORIMOTO, N., 1989. Nomenclature of pyroxenes. The Canadian Mineralogist, 27, p. 143-156.

MORTENSEN, J.K., GHOSH, D. and FERRI, F., 1995. U-Pb geochronology of intrusive rocks associated with copper-gold porphyry deposits in the Canadian Cordillera. *In* Porphyry Deposits of the Northwestern Cordillera of North America. *Edited by* T.G. Schroeter. Canadian Institute of Mining, Metallurgy and Petroleum, Special Volume 46.

MORTIMER, N., 1987. The Nicola Group: Late Triassic and Early Jurassic subduction-related volcanism in British Columbia. Canadian Journal of Earth Sciences, 24, p. 2521-2536.

NANEY, M. T., 1983. Phase equilibria of rock-forming ferromagnesian silicates in granitic systems. American Journal of Science, 283, p. 993-1033.

NICHOLLS, J. and RUSSELL, J.K., 1991. Major-element chemical discrimination of magma-batches in lavas from Kilauea Volcano, Hawaii, 1954-1971 eruptions. Canadian Mineralogist, 29, p. 981-993.

NORTHCOTE, K.E., 1974. Geology of the northwest half of the Iron Mask Batholith. *In* Geological Fieldwork 1974. British Columbia Ministry of Energy, Mines and Petroleum Resources, Paper 1975-1, p. 22-26.

NORTHCOTE, K.E., 1976. Geology of the southeast half of the Iron Mask Batholith. *In* Geological Fieldwork 1976. British Columbia Ministry of Energy, Mines and Petroleum Resources, Paper 1977-1, p. 41-46.

NORTHCOTE, K.E., 1977. Iron Mask Batholith. British Columbia Ministry of Energy, Mines and Petroleum Resources, Preliminary Map 26 and accompanying notes, 8 p.

PEARCE, T.H., 1968. A contribution to the theory of variation diagrams. Contributions to Mineralogy and Petrology, 19, p. 142-157.

PEARCE, J.A., HARRIS, N.B.W. and TINDLE, A.G., 1984. Trace element discrimination diagrams for the tectonic interpretation of granitic rocks. Journal of Petrology, 25, p. 956-983.

PRETO, V.A., 1967. Geology of the eastern part of the Iron Mask Batholith. British Columbia Ministry of Mines and Petroleum Resources, Annual Report 1967, p.137-147.

PRETO, V.A., 1972. Afton, Pothook. *In* Geology, Exploration and Mining in British Columbia. British Columbia Ministry of Energy, Mines and Petroleum Resources, p. 209-220.

PRETO, V.A., 1977. The Nicola Group: Mesozoic volcanism related to rifting in southern British Columbia. *In* Volcanic Regimes in Canada. *Edited by* W.R.A. Baragar, L.C. Coleman and J.M. Hall. The Geological Association of Canada, Special Paper No. 16, p. 39-57.

PRETO, V.A., 1979. Geology of the Nicola group between Merritt and Princeton. British Columbia Ministry of Energy, Mines and Petroleum Resources, Bulletin 69, 90 p.

ROSS, K.V., DAWSON, K.M., GODWIN, C.I. and BOND, L., 1993. Major lithologies and alteration of the Ajax East orebody, a subalkalic Copper-Gold Porphyry Deposit, Kamloops, South Central British Columbia. *In* Current Research 1993. Geological Survey of Canada, Paper 93-1A, p. 87-95.

ROSS, K.V., GODWIN, C.I., BOND, L. and DAWSON, K.M., 1995. Geology, alteration and mineralization in the Ajax East and Ajax West deposits, southern Iron Mask batholith, Kamloops, British Columbia. *In* Porphyry Deposits o. lorthwestern Cordillera of North America. *Edited by* T.G. Schroete.. Canadian Institute of Mining, Metallurgy and Petroleum, Special Volume 46.

RUSSELL, J.K. and NICHOLLS, J., 1988. Analysis of petrologic hypotheses with Pearce element ratios. Contributions to Mineralogy and Petrology, 99, p. 25-35.

RUSSELL, J.K. and SNYDER, L.D., 1993a. Volatile production possibilities during magmatic assimilation. *In* Volcanoes and ore Deposits. Mineral Deposit Research Unit, The University of British Columbia, Vancouver, British Columbia, Short Course No. 14 Notes.

RUSSELL, J.K. and SNYDER, L.D., 1993b. Volatile production attending magmatic assimilation processes. *In* Ancient Volcanism and Modern Analogues. IAVCEI General Assembly, Canberra, Australia, p. 94.

SCHAU, M., 1970. Stratigraphy and structure of the type area of the Upper Triassic Nicola Group in south-central British Columbia. Geological Association of Canada, Special Paper No. 6, p. 123-135.

SCOTT, P.W., 1976. Crystallization trends of pyroxenes from the alkaline volcanic rocks of Tenerife, Canary Islands. Mineralogical Magazine, 40, p. 805-816.

SNYDER, L.D., 1994. Petrological studies within the Iron Mask batholith, south central British Columbia. Unpublished M.Sc. thesis, The University of British Columbia, Vancouver, British Columbia, 192 p.

SNYDER, L.D. and RUSSELL, J.K., 1993. Field constraints on diverse igneous processes in the Iron Mask Batholith (92I/9, 10). *In* Geological Fieldwork 1992. *Edited by* B. Grant and J.M. Newell. British Columbia Ministry of Energy, Mines and Petroleum Resources, Paper 1993-1, p. 281-286.

SNYDER, L.D. and RUSSELL, J.K., 1994. Petrology and stratigraphic setting of the Kamloops Lake picritic basalts, Quesnellia Terrane, South-Central B.C. (92I/9, 15 and 16). *In* Geological Fieldwork 1993. *Edited by* B. Grant and J.M. Newell. British Columbia Ministry of Energy, Mines and Petroleum Resources, Paper 1994-1, p. 297-311.

STANLEY, C.R., 1994. Geology of the Pothook alkalic copper-gold porphyry deposit, Afton Mining Camp, British Columbia (92I/9, 10). *In* Geological Fieldwork 1993. *Edited by* B. Grant and J.M. Newell. British Columbia Ministry of Energy, Mines and Petroleum Resources, Paper 1994-1, p. 275-284.

STANLEY, C.R. and RUSSELL, J.K., 1989. Petrologic hypothesis testing with Pearce element ratio diagrams; derivation of diagram axis. Contributions to Mineralogy and Petrology, 103, p. 78-89.

STANLEY, C.R., LANG, J.R. and SNYDER, L.D., 1994. Geology and mineralization in the northern part of the Iron Mask Batholith, British Columbia (92I/9, 10). *In* Geological Fieldwork 1993. *Edited by* B. Grant and J.M. Newell. British Columbia Ministry of Energy, Mines and Petroleum Resources, Paper 1994-1, p. 269-274.

THORNTON, C.P. and TUTTLE, O.F., 1960. Chemistry of igneous rocks — Pt 1, differentiation index. American Journal of Earth Science, 258, p. 664-684.

WATSON, E.B. and HARRISON, T.M., 1983. Zircon saturation revisited: Temperature and composition effects in a variety of crustal magma types. Earth and Planetary Science Letters, 64, p. 295-304.

WATSON, E.B. and HARRISON, T.M., 1984. Accessory minerals and the geochemical evolution of crustal magmatic systems: A summary and prospectus of experimental approaches. Physics of the Earth and Planetary Interiors, 35, p. 19-30.